Functional properties of habenular neurons are determined by developmental stage and sequential neurogenesis

Stephanie Fore[1], Francisca Acuña-Hinrichsen[1], Kadir Aytac Mutlu[1], Ewelina Magdalena Bartoszek[1], Bram Serneels[1], Nicholas Guy Faturos[1], Khac Thanh Phong Chau[1], Mehmet Ilyas Cosacak[2], Carmen Diaz Verdugo[1], Fabrizio Palumbo[1], Christa Ringers[1], Nathalie Jurisch-Yaksi[1,3,4], Caghan Kizil[2,5], Emre Yaksi[1*]

1Kavli Institute for Systems Neuroscience and Centre for Neural Computation, Faculty of Medicine and Health Sciences, Norwegian University of Science and Technology, Olav Kyrres gata 9, 7030 Trondheim, Norway.
2German Center for Neurodegenerative Diseases (DZNE) Dresden, Helmholtz Association, Tatzberg 41, 01307, Dresden, Germany.
3Department of Clinical and Molecular Medicine, Norwegian University of Science and Technology, Olav Kyrres Gate 9, 7030 Trondheim
4Department of Neurology and Clinical Neurophysiology, St Olav University Hospital, Edvard Griegs Gate 8, 7030 Trondheim, Norway
5Center for Molecular Cell Biology (CMCB), TU Dresden, Fetscherstr. 105, 01307, Dresden, Germany
*Corresponding author: emre.yaksi@ntnu.no

SUMMARY

Neural development is not just a linear expansion of the brain. Instead, the structure and function of developing brain circuits undergo drastic alterations that have a direct impact on the animals' expanding behavioural repertoire. Here we investigated the developmental changes in the habenula, a brain region that mediates behavioural flexibility during learning, social interactions and aversive experiences. We showed that developing habenular circuits exhibit multiple alterations, that lead to an increase in the structural and functional diversity of cell types, inputs and functional modules within habenula. As the neural architecture of the habenula develops, it sequentially transforms into a multi-sensory brain region that can process visual, olfactory, mechanosensory and aversive stimuli. Moreover, we also observed that already at early developmental stages, the habenular neurons display spatio-temporally structured spontaneous activity that shows prominent alterations and refinement with age. Interestingly, these alterations in habenular activity are accompanied by sequential neurogenesis and the integration of distinct neural clusters across development. Finally, by combining an in vivo neuronal birthdating method with functional imaging, we revealed that habenular neurons with distinct functional properties are born sequentially at distinct developmental time windows. Our results highlight a strong link between the functional properties of habenular neurons and their precise birthdate during development.

INTRODUCTION

During development and maturation, the functional capacity of brain circuits increases in order to support the animals' expanding behavioural repertoire. For example, while a young zebrafish larvae mostly needs to avoid threats [1-3] and find food [4], more cognitively demanding behaviours such as associative learning [5-7] or social interactions [8, 9] emerge later in development during the juvenile stage around 3-4 weeks. Such an expansion of the behavioural repertoire is a feature that is conserved across vertebrates [10, 11], and is often accompanied with the development, establishment and maturation of distinct circuit components generating functional modules within the brain [12-14]. Hence, brain development and maturation is not just a linear expansion of the already existing building blocks, but also a sequential increase in the diversity of functional modules and cell types. In the cortex, for example, individual layers are born at different time points, with deep layers being born earlier than superficial layers [15-17], creating a diversity in the cytoarchitecture of cortical layers and regions with distinct functions [12, 18-20]. Similarly, such chronological order of neurogenesis in larval zebrafish hindbrain and spinal cord was shown to generate functional diversity of neurons, which underlies increased sophistication of behaviours across development [21-24].

The maturation and refinement of the developing brain rely on neural activity that can be evoked by sensory inputs [25, 26], or spontaneously generated [25, 27-30]. In most sensory systems, sensory evoked activity was shown to be critical for the maturation of neural circuits and the refinement of topographical maps [26, 31-34]. The appearance of spontaneous activity of the developing brain starts early, and coincides with periods of intense synaptogenesis and neuronal growth [29, 35, 36]. For example, spontaneous activity bursts were observed in the visual, auditory and somatosensory systems [37, 38], and are shown to be important for the remodelling of these structures [30, 31, 39]. In higher brain regions, such as the hippocampus, large and slow bursts are observed [40, 41] before the appearance of faster rhythms and the patterned activity of the adult hippocampus associated with learning and memory [41, 42]. Furthermore, spontaneous activity is also involved in the maturation of connections across distant brain regions, as observed between the olfactory bulb and the entorhinal cortex [43]. Finally, the synchronous bursting during spontaneous activity that is important in establishing neural connectivity

[44, 45], was shown to be mediated via excitatory connections [46, 47], gap junctions [48], glia [49], or other support cells [50]. Taken together, both sensory-driven and spontaneous neural activity are essential in the development and maturation of neural circuits. It is, however less clear how sensory evoked and spontaneous neural activity interact, as the animals develop.

While the majority of studies have focused on the development of sensory and motor systems, less is known about the maturation of higher brain areas integrating information from multiple brain regions, such as the habenula. The habenula is a particularly interesting brain region, as it was shown to integrate both sensory [51-53] and cortico-limbic inputs [54-62] while directly regulating the function of monoaminergic brain nuclei controlling behaviour [53, 57, 63-67]. Dysfunction of the habenula is also shown to be associated with several neurological conditions and mood disorders including depression [68, 69]. The habenula is composed of several subdomains or modules based on its neurochemical profiles [70-75], anatomical projections [76-79] and the activity of habenular neurons [79-81]. Two major subnuclei, the lateral and medial habenula in mammals, respectively dorsal habenula (dHb) and ventral habenula (vHb) in zebrafish, have clear differences in their functional and molecular profiles [77, 79]. While the dHb is involved in sensory processing [53, 65], circadian rhythms [65], aggression [82] and experience-dependent fear response [63, 76, 77], the vHb was shown to play a role in avoidance learning [79] and active coping behaviour [83]. In zebrafish, dHb and vHb originate from separate neural progenitor pools and were suggested to maturate at distinct developmental time points [84]. Moreover, the dHb was shown to undergo asymmetric neurogenesis during the early stages of development, with left dHb neurons being born earlier than the ones in the right hemisphere [85]. The prominent asymmetry in the molecular [71] and anatomical properties of habenula [86, 87], is also reflected in its asymmetric encoding of visual and olfactory information in the left and the right dHb hemispheres respectively [51, 80, 81]. Recent transcriptome analysis further revealed multiple molecularly distinct and spatially organized functional modules within the zebrafish [73] and mammalian[88] habenula, which resemble the spatially organized functional clusters of habenular neurons during spontaneous activity [81]. All of these evidences suggest a fine spatial organization of distinct functional modules within habenula [81]. In addition, spontaneous habenular activity was shown to govern sensory responses and therefore proposed to represent internal states of the network, which could mediate the selection of appropriate behaviours [81]. In fact, a recent study revealed a sequential recruitment of neurons generating an increase in vHb activity, during the switch from active to passive coping behaviours in juvenile zebrafish [83]. Interestingly, such complex behaviours emerge at later stages of zebrafish development [5, 6, 8, 9], suggesting pronounced changes in the underlying circuitry across the brain. Despite extensive characterization of habenular circuitry during very early developmental stages [71, 85, 86], it is still unclear how the maturation of habenular networks during development, corresponds to the establishment of its distinct functional modules. In this study, we investigated how the function and the architecture of habenular networks change across development, and how these alterations relate to the formation of distinct functional modules within habenula. We showed that as the habenula expands, the number of neurons increases, inhibitory connections are formed and sensory inputs are integrated with a temporal order. Moreover, we revealed that the habenula is a multi-sensory brain region, which distinctly encodes different sensory modalities. Visual and olfactory responses in habenula develop early while the responses to mechanosensory and aversive stimuli develop at later stages. Spontaneous habenular activity is present already at early developmental stages and it is predictive of the habenular neurons with sensory responses. Interestingly, we observed a prominent restructuring of both spatial and temporal features of spontaneous habenular activity during development. These functional changes in the habenula were accompanied by a sequential and spatially organized addition of newly born neurons across development. Finally, we showed that habenular neurons born at a distinct developmental stage, exhibit similar functional properties. Our observations support the idea that neuronal birthdate and function are strongly related.

RESULTS

New neurons and new inhibitory connections are added to habenula during development

To study the functional development of zebrafish habenula, we focused on three developmental stages: early larval stage-3dpf (days post fertilization), late larval stage-6dpf and juvenile stage-21dpf. During these periods, zebrafish transition from self-feeding larvae (via the yolk sac) to an external feeding juvenile animal with more complex behaviours including those involving habenular circuits [5, 8, 9, 76, 79, 83]. First, we visualized the gross morphology of habenula in Tg(elavl3:GCaMP6s) [89] zebrafish, labelling most habenular neurons. We observed that the number of habenular neurons increases drastically from 3 to 21 days of zebrafish development (Figure 1A-B). Next we investigated the expression of glutamate and GABA by using Tg(vglut2a:dsRed) [51] and Tg(gad1b:GFP) [90] zebrafish. We found that at 3dpf, habenula mainly consists of glutamatergic neurons, and as the

animal gets older few GABAergic neurons are added (Figure 1C). Interestingly, from 6dpf on we also observed prominent bilateral GABAergic projections that innervate specific domains at the lateral sides of habenula (Figure 1C). These results suggest that habenula undergoes a non-linear expansion with the addition of new cell types and inputs arriving at different time points throughout development.

Sensory inputs and computations in habenula follow a developmental order

Previous studies showed that habenula receives olfactory [51] and visual [52, 53] inputs and responds to both of these sensory modalities [64, 80, 81]. To investigate how these sensory inputs maturate during habenula development, we visualized the mitral cell and thalamic axon terminals in habenula using Tg(lhx2a:gap-YFP) [51] and Et(-0.6hsp70l:Gal4-VP16) s1020t ; Tg(UAS:nfsB-mCherry) [76, 91, 92] zebrafish lines, respectively. At all ages, thalamic projections were found to innervate habenula (Figure 2A, blue) in distinct locations that are different from GABAergic innervations (Figure 2A, white) or mitral cell terminals (Figure 2A, red). Yet, the density of olfactory bulb projections increased with age (Figure 2A, red). These findings suggest that habenular neurons may be predominantly light responsive at younger ages, while odour responses develop later. To test this hypothesis, we measured odour (food odour) and light (red light flash) responses in the habenula by using two-photon calcium imaging in Tg(elavl3:GCaMP6s) [89] zebrafish. At 3dpf we found that a significantly higher portion of habenular neurons responds to the visual stimulus compared to food odour (Figure 2B-C). As zebrafish develop, the ratio of odour and light responding neurons became similar (Figure 2B-C). To further test whether the development of sensory responses in habenula is biased towards aversive or attractive stimuli within one sensory modality, we applied two attractive and two aversive odours [81]. We observed that habenular neurons develop a stronger preference for aversive odours, compared to attractive odours during the juvenile stage (supplementary Figure 1). At all developmental stages, correlations between visual vs olfactory (Figure 2D), or between aversive and attractive olfactory stimuli were relatively low (supplementary Figure 1).

Previous studies showed that the zebrafish habenula can encode a diverse range of aversive experiences [63, 73, 83]. To test the developmental order of zebrafish habenula for encoding aversive stimuli, we applied mechanical vibrations [1] and mild electric stimulation [63, 73, 83], and compared these responses to visual responses evoked by red light. Consistent with our results above, the zebrafish habenula predominantly responds to visual stimulation at 3dpf (Figure 3A-B). As zebrafish develop, we observed that habenular neurons first exhibit more prominent responses to mild-electric stimulation at 6dpf, and later also to mechanical vibrations at 21dpf (Figure 3A-B). These three different stimulus modalities,

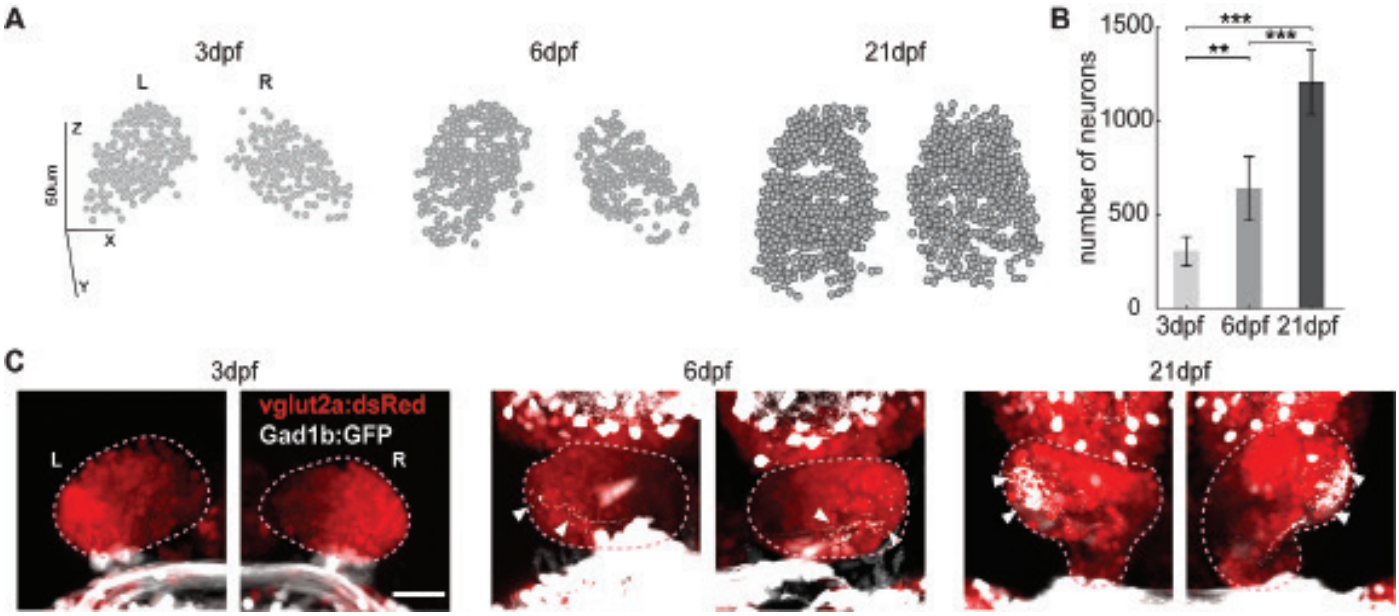

Figure 1: During development the number of habenular neurons increases and new GABAergic connections are added

(A) Representative examples of three-dimensional reconstructions of habenular neurons detected in Tg(elavl3:GCaMP6s) zebrafish line, using volumetric two-photon calcium imaging at three different developmental ages (3, 6 and 21dpf). Coronal view.

(B) The average number of neurons detected in Tg(elavl3:GCaMP6s) at 3dpf (n=9 fish), 6dpf (n=6 fish) and 21dpf (n=9 fish), **p<0.01, ***p<0.001, t-test. Data presented as mean ±SEM.

(C) Confocal microscopy projections of habenula in Tg(vglut2a:dsRed) and Tg(gad1b:GFP) double transgenic zebrafish at 3,6 and 21dpf, labelling glutamatergic (red) and GABAergic (white) neurons and projections, dorsal view. White arrows indicate GABAergic projections. White scale bar represents 100µm. L,left; R,right hemisphere.

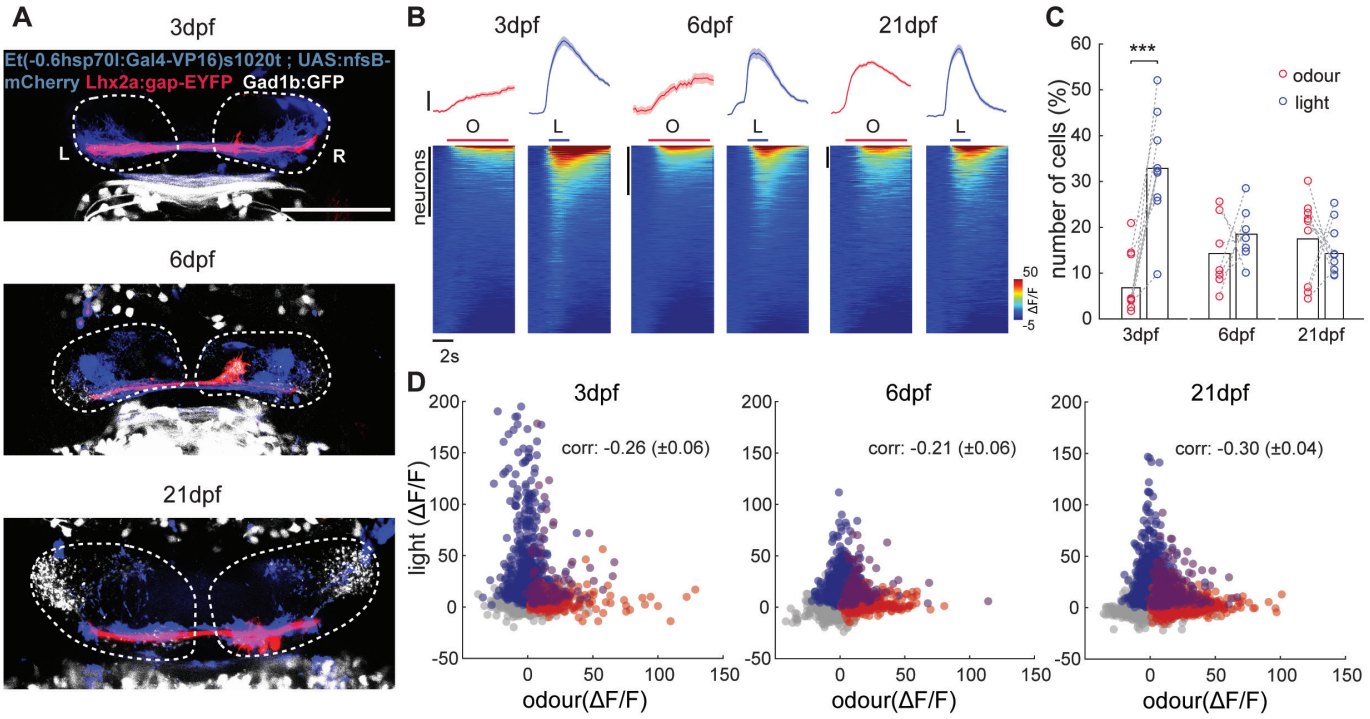

Figure 2: Visual responses dominate larval habenula, while olfactory responses develop later
(A) Confocal microscopy projections of habenula in Tg(Lhx2:gap-YFP) ; (Et(0.6hsp70l:Gal4-VP16) s1020t ; Tg(UAS:nfsB-mCherry) and Tg(gad1b:GFP) triple transgenic zebrafish labelling olfactory bulb projections (red), thalamic projections (blue) and GABAergic projections (white), dorsal view. Dashed white lines delineate habenula. White bar represents 100μm. L,left; R,right hemisphere. (B) Top panel shows average responses of odour-responding (red) and light-responding habenular neurons (blue) over 4-5trials at 3dpf (n=9), 6dpf (n=7) and 21dpf (n=9) zebrafish. Black bars represent 10% ΔF/F. Shadows represent SEM. Bottom panel shows colour coded sensory responses (ΔF/F) of all individual Hb neurons exposed to 5s odour (O, red) stimulus (left) and 2s light (L, blue) stimulus (right) in all fish imaged at 3,6 and 21dpf. Black bars represent 1000 neurons. (C) Percentage of odour (red dots) vs light (blue dots) responding neurons at 3,6 and 21dpf. ***p<0.001 paired t-test. All data presented as mean ±SEM. (D) Odour (red) vs light (blue) response amplitude of all habenular neurons responses at 3,6 and 21dpf. Magenta colour depicts the neurons responding to both odour and light. Grey dots represents non-responsive neurons. Average±SEM correlations between different stimulus representations by habenular responses are represented by "corr". Note that at all ages odour and light responses are dissimilar, depicted by the negative correlations.

exhibit low correlations at all developmental stages (Figure 3C). Taken together, these results suggest that the developing habenula can selectively encode an expanding number of sensory modalities with an increasing preference for aversive stimuli at later stages.

Functional lateralization of visual and olfactory responses decreases across development, and it is not prominent for aversive stimuli

Earlier studies revealed a strong molecular [71, 72, 77, 78] and functional [64, 80] lateralization of habenular networks especially across the dHb hemispheres of larval zebrafish. Interestingly, there is no evidence for such lateralization in the rodent habenula, which is mostly studied in adults by using aversive stimuli [55, 57, 59]. This made us question whether the ontogeny of functional lateralization in the zebrafish habenula might resemble the phylogeny of the vertebrate habenula, where lateralized responses to light and odours appear first and nonlateralized responses to aversive stimuli develop later. To test this hypothesis we investigated the lateralization of sensory responses in habenular neurons across zebrafish development. First, we showed that the dorsal sections of habenula, which likely cover the dHb, exhibit lateralized visual and olfactory responses at all ages (Figure 4A-B). We quantified this functional lateralization by measuring the ratio of light vs odour responding habenular neurons across hemispheres [80] and by using a lateralization index, where 0 represent symmetry and 1 represent complete segregation of light and odour responses across hemispheres. Across development, dHb exhibits high functional lateralization of light and odour responses, when compared to the ventral sections of habenula (Figure 4B). Yet, we also observed that the functional lateralization of habenular circuits significantly decreases across development (Figure 4C-D). Despite this decrease, light and odour responses exhibit prominent spatial organization (Figure 4E), quantified by the focality index, ranging from 0 (for random spatial distribution of sensory responses) to 1 (for maximally focal sensory responses) [93]. Instead, aversive stimuli elicited no such lateralization across habenular hemispheres (supplementary Figure 2), resembling the non-lateralized aversive cue representations in the rodent habenula [55, 57, 59]. These results indicate that functional lateralization is a feature of dHb [80] that develops earlier and preferentially responds to

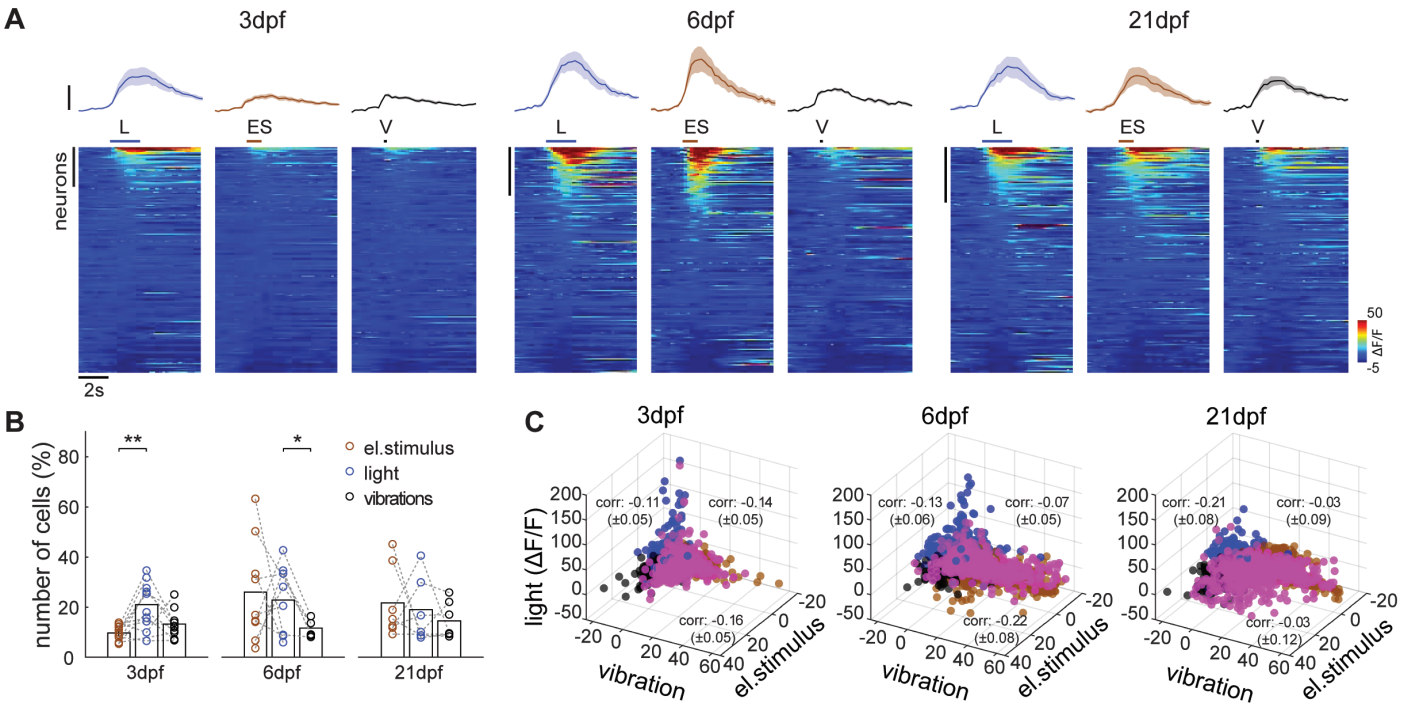

Figure 3: Habenular neurons encode aversive stimuli during later developmental stages.
(A) Top panel shows average responses in habenular neurons to light (L, blue), mild electric stimulation (ES, brown) and mechanical vibrations (V, black) over 4-5trials in at 3dpf (n=11), 6dpf (n=9) and 21dpf (n=7) zebrafish. Black bars represent 10% ΔF/F. Shadows represent SEM. Bottom panel shows colour coded sensory responses (ΔF/F) of all individual Hb neurons exposed to 2s light stimulus (left), 1s mild electric stimulation (middle) and 0.05s mechanical vibration (right) in all fish imaged at 3,6 and 21dpf. Black bars represent 1000 neurons. (B) Percentage of responding neurons to light (blue), mild electric stimulus (brown), mechanical vibrations (black) at 3,6 and 21dpf. *p<0.05 **p<0.01 paired t-test. (C) Light (blue) vs mild electric stimulus (brown) vs mechanical vibrations (black) response amplitude of all habenular neurons responses at 3,6 and 21dpf. Magenta colour depicts the neurons responding to more than one stimuli. Average±SEM correlations between different stimulus representations by habenular responses are represented by "corr". Note that at all ages different stimulus modalities are distinctly represented, depicted by the negative correlations. All data presented as mean ±SEM.

visual and olfactory stimuli. Instead, vHb, which develops later during development, does not exhibit prominent functional lateralization.

Functional clusters of habenular neurons exhibit spatially organized spontaneous activity at all ages

IOurresultsrevealedthatalreadyatearlydevelopmental stages, the habenula exhibits prominent spontaneous activity. In several brain regions, spontaneous activity during early development is generally characterized as large bursts with long quiescent intervals [37, 38, 40], whereas adult brains usually exhibit rhythmic activity at faster frequencies [40, 94]. To test whether the temporal features of habenular activity are changing over development, we detected the spontaneous activity bursts [95] (Figure 6A) and quantified the frequency and duration of these events. We observed that as the animals develop, the frequency of spontaneous activity bursts significantly increases (Figure 6B) and their duration decreases (Figure 6C). Moreover, while the average activity of habenular neurons decreases (Figure 6D), a larger proportion of habenular neurons shows spontaneous activity (Figure 6E) at later developmental stages. These results are in line with the developmental changes observed in other vertebrate brain regions and highlight the maturation of habenular spontaneous activity across development.

Next, we asked whether such temporal features (i.e. burst duration and frequency) of spontaneous habenular activity are also spatially organized. We quantified the spatial distribution by using the measure of focality index, ranging from 0 (for random spatial distribution) to 1 (for an extremely focal point) [93]. At all developmental stages the temporal features of habenular spontaneous activity, burst frequency, and duration were highly focal and not randomly distributed (Figure 6F, also note the mean focality values). To further investigate the spatial distribution of habenular activity at different developmental stages, we adopted a commonly used reporter of neural activity, phospho-ERK/total-ERK (pERK/tERK) ratio [96-98]. We observed that during early developmental stages pERK/tERK ratio is distributed rather uniformly across the habenula (Figure 6G-H top), while at later developmental stages pERK/tERK ratio was concentrated more laterally (Figure 6G-H bottom), indicating a higher neural activity towards the lateral ends of habenula. Interestingly we also observed that the most silent habenular neurons (black dots in Figure 5F), were located closer to the medial wall of habenula (Figure 6I), near the location of habenular neural progenitors labelled in Tg(her4.1:GFP) [99] zebrafish (Figure 7A).

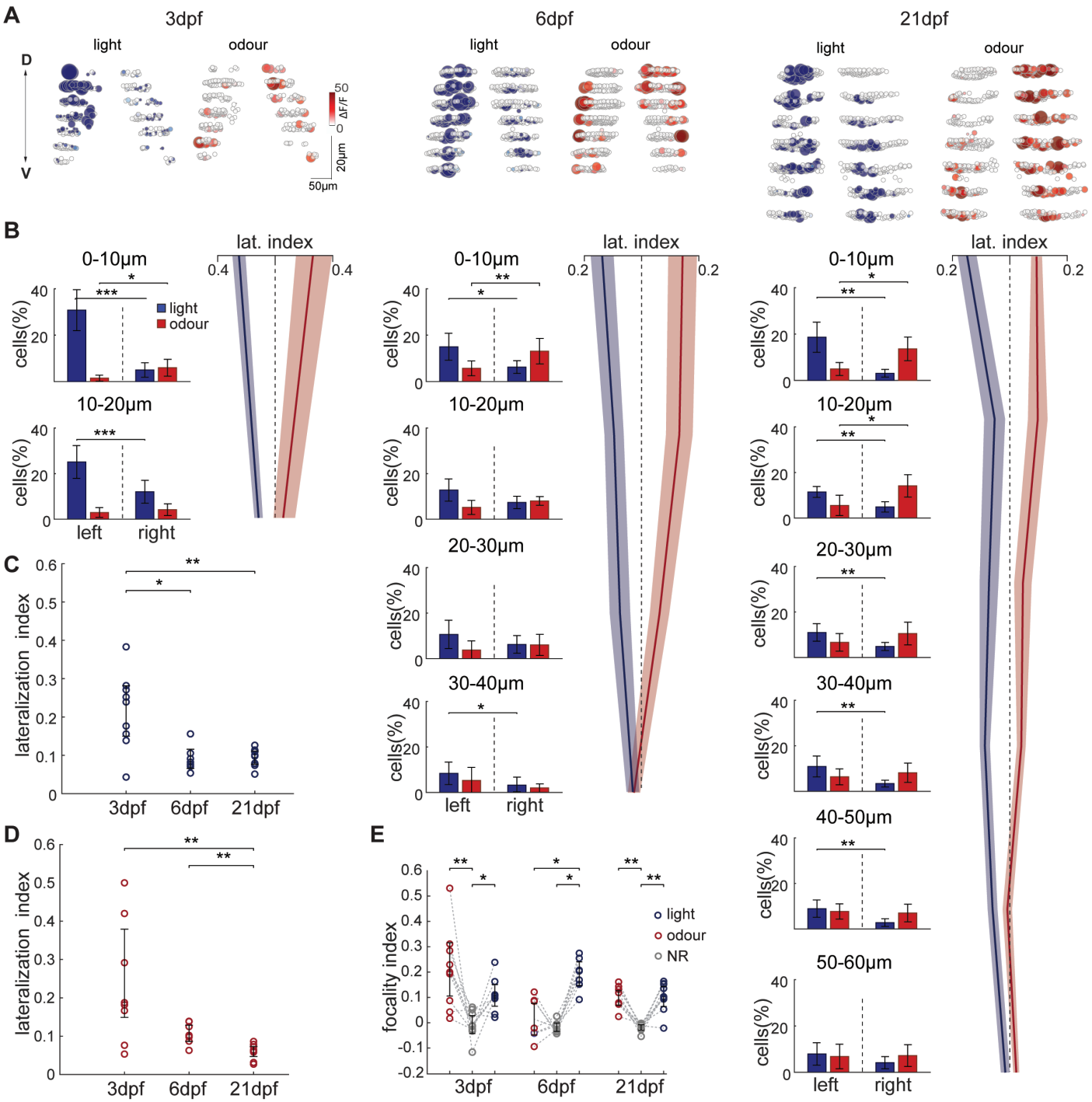

Figure 4: Sensory lateralization is prominent in dorsal habenula at all ages, but decreases with age especially in ventral habenula.

(A) Three-dimensional reconstructions of habenular responses to light (blue) and odour (red) stimulation recorded by volumetric two-photon microscopy in Tg(elavl3:GCaMP6s) zebrafish, at 3,6 and 21dpf. White dots indicates non-responding neurons. Coronal view. (B) The ratio of odour (red) vs light (blue) responding neurons in left vs right habenular hemispheres, as well as associated sensory lateralization index at 3 (left), 6 (middle) and 21 (right) dpf zebrafish. Each row represents the average values for neurons within 10μm plane (from the top to bottom). Shades represent the ±SEM. 3dpf (n=9 fish), 6dpf (n=7 fish) and 21dpf (n=9 fish). *p<0.05, **p<0.01, ***p<0.001, t-test. (C) Average lateralization index of light responses for the entire habenula of all fish at 3,6 and 21dpf. *p<0.05, **p<0.01, Wilcoxon ranksum test. (D) Average lateralization index of odour responses for the entire habenula of all fish at 3, 6 and 21dpf. **p<0.01, Wilcoxon ranksum test. (E) Focality index for odour (red) and light (blue) responding neurons compared to NR (non-responding neurons, gray) at 3, 6 and 21dpf. **p<0.01, ***p<0.001, Wilcoxon signed-rank test. All data presented as mean ±SEM.

Since the juvenile zebrafish habenula displayed an increased pERK/tERK ratio towards the lateral ends (Figure 6G-H) and a higher number of silent neurons towards the medial ends (Figure 6I), we hypothesized that the mediolateral distribution of habenular neurons at older stages might represent their physiological and developmental maturity. To test this hypothesis, we performed intracellular recordings of habenular neurons across the mediolateral axis of juvenile zebrafish at later developmental stages. In fact, we

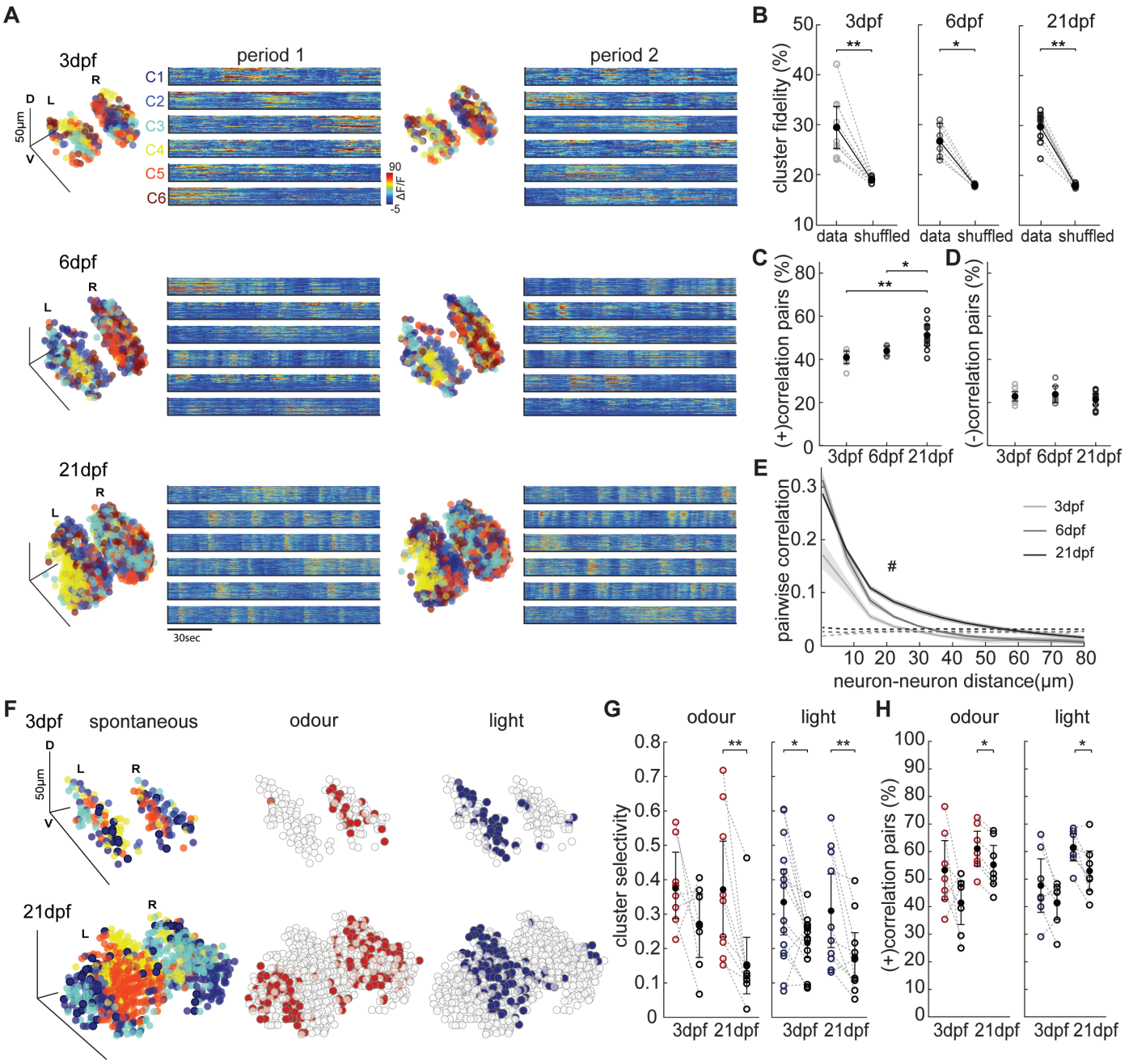

Figure 5: Spontaneous habenular activity is structured into spatially organized functional clusters of neurons that are preserved during sensory responses, at all ages.

(A) Functional clusters of habenular neurons with synchronous spontaneous activity in two different time periods (period 1 and period 2). Three-dimensional reconstruction depicts the spatial locations of all neurons. Each colour represents a neuronal cluster with similar spontaneous activity, defined by using k-means clustering. Colour coded neural traces on the right, show the spontaneous activity of each neuron that belongs to a given cluster "C". warm colour represents increased neural activity. Each row represents an example zebrafish at 3, 6 and 21dpf. (B) Cluster fidelity, depicting the ratio of neural pairs that remain within the same functional cluster during 2 different time periods for 3dpf (n=9), 6dpf (n=6) and 21dpf (n=9), compared to shuffled chance levels. *p<0.05, **p<0.01, Wilcoxon signed-rank test. (C) The ratio of neural pairs with significant (p<0.05) positive correlations during two periods of spontaneous activity. *p<0.05, **p<0.01, Wilcoxon ranksum test. (D) The ratio of neural pairs with significant (p<0.05) negative correlations during two periods of spontaneous activity. Wilcoxon ranksum test. (E) Relation between pairwise correlation of spontaneous neural activity and the distance between each neuron pair in habenula at 3, 6 and 21dpf. Dotted lines represent the results when neuron locations are shuffled. ANOVA-n displayed significance over distances (p<0.001) and over age groups (p<0.001) indicated with #. (F) Colour coded functional clusters of habenular neurons with synchronous spontaneous activity for an example zebrafish at 3 (top) and 21(bottom) dpf. On the middle and right panels, odour (red) and light (blue) responses of the same neurons are visualized. Scale bars represent 50μm. (G) Cluster selectivity, depicting how odour (red) or light (blue) responding neurons are distributed into functional clusters based on their spontaneous activity. High selectivity means that both odour and light responding neurons belong to fewer clusters compared to the same number of randomly selected non-sensory neurons (grey dots), at 3 and 21dpf. (H) The ratio of neural pairs with significant (p<0.05) positive correlations of spontaneous activity, for odour and light responsive neurons, when compared to the same number of randomly selected non-sensory neurons, at 3 and 21dpf. *p<0.05, **p<0.01, ***p<0.001, Wilcoxon signed-rank test. All data presented as mean ±SEM.

observed that the input resistance, a hallmark of developmental maturation of cortical neurons [20, 100], was significantly higher for medial habenular neurons, compared to lateral habenular neurons(Figure 6J). Taken together this suggests that neurons near the lateral ends of habenula might be more mature neurons that are born during early developmental stages, compared to medial habenula neurons born later.

Features of spontaneous habenular activity change during development

Our results revealed that already at early developmental stages, the habenula exhibits prominent spontaneous activity. In several brain regions, spontaneous activity during early development is generally characterized as large bursts with long quiescent intervals [37, 38, 40], whereas adult brains usually exhibit rhythmic activity at faster frequencies [40, 94]. To test whether the temporal features of habenular activity are changing over development, we detected the spontaneous activity bursts [95] (Figure 6A) and quantified the frequency and duration of these events. We observed that as the animals develop, the frequency of spontaneous activity bursts significantly increases (Figure 6B) and their duration decreases (Figure 6C). Moreover, while the average activity of habenular neurons decreases (Figure 6D), a larger proportion of habenular neurons shows spontaneous activity (Figure 6E) at later developmental stages. These results are in line with the developmental changes observed in other vertebrate brain regions and highlight the maturation of habenular spontaneous activity across development.

Next, we asked whether such temporal features (i.e. burst duration and frequency) of spontaneous habenular activity are also spatially organized. We quantified the spatial distribution by using the measure of focality index, ranging from 0 (for random spatial distribution) to 1 (for an extremely focal point) [93]. At all developmental stages the temporal features of habenular spontaneous activity, burst frequency, and duration were highly focal and not randomly distributed (Figure 6F, also note the mean focality values). To further investigate the spatial distribution of habenular activity at different developmental stages, we adopted a commonly used reporter of neural activity, phospho-ERK/total-ERK (pERK/tERK) ratio [96-98]. We observed that during early developmental stages pERK/tERK ratio is distributed rather uniformly across the habenula (Figure 6G-H top), while at later developmental stages pERK/tERK ratio was concentrated more laterally (Figure 6G-H bottom), indicating a higher neural activity towards the lateral ends of habenula. Interestingly we also observed that the most silent habenular neurons (black dots in Figure 5F), were located closer to the medial wall of habenula (Figure 6I), near the location of habenular neural progenitors labelled in Tg(her4.1:GFP) [99] zebrafish (Figure 7A).

Since the juvenile zebrafish habenula displayed an increased pERK/tERK ratio towards the lateral ends (Figure 6G-H) and a higher number of silent neurons towards the medial ends (Figure 6I), we hypothesized that the mediolateral distribution of habenular neurons at older stages might represent their physiological and developmental maturity. To test this hypothesis, we performed intracellular recordings of habenular neurons across the mediolateral axis of juvenile zebrafish at later developmental stages. In fact, we observed that the input resistance, a hallmark of developmental maturation of cortical neurons [20, 100], was significantly higher for medial habenular neurons, compared to lateral habenular neurons(Figure 6J). Taken together this suggests that neurons near the lateral ends of habenula might be more mature neurons that are born during early developmental stages, compared to medial habenula neurons born later.

Distinct spatial domains of habenular neurons are born through sequential neurogenesis

Next, we asked whether the spatial organization of habenula across the mediolateral axis might be a result of sequential neurogenesis across development. To tests this hypothesis, we first investigated the location of habenular neurogenesis. We observed that neural progenitors labelled by Tg(her4.1:GFP) [99] expression are located at the medial walls of habenular hemispheres (Figure 7A). To further investigate the relationship between the birthdate of habenular neurons and their spatial distribution, we labelled habenular neurons born during different developmental stages using BrdU incorporation (Figure 7B). BrdU birthdating showed that the habenular neurons that are born during distinct developmental stages were spatially organized (Figure 7C). Moreover, we observed that the birthdate of habenular neurons is a good indicator for their spatial location, where oldest neurons (born early in development) mostly occupied the lateral wall of habenula, and youngest neurons (born late in development) were closest to the medial wall (Figure 7C-D).

Next, we developed an in vivo birthdating method to further investigate the distinct clusters of habenular neurons that are born during different developmental stages. To do this, we adopted a previously described approach to label cohorts of mammalian cortical neurons born at distinct developmental stages [101]. We achieved this by injecting two different colours (far-red and green) of a fluorescent cell tracer in the telencephalic ventricle [102], near the neural progenitor zone on the medial wall of habenula (Figure 7A) of 2,5dpf and 5dpf zebrafish larvae (Figure 7E). 15 hrs after the cell tracer injections, only the cells near the medial wall of habenula were labelled

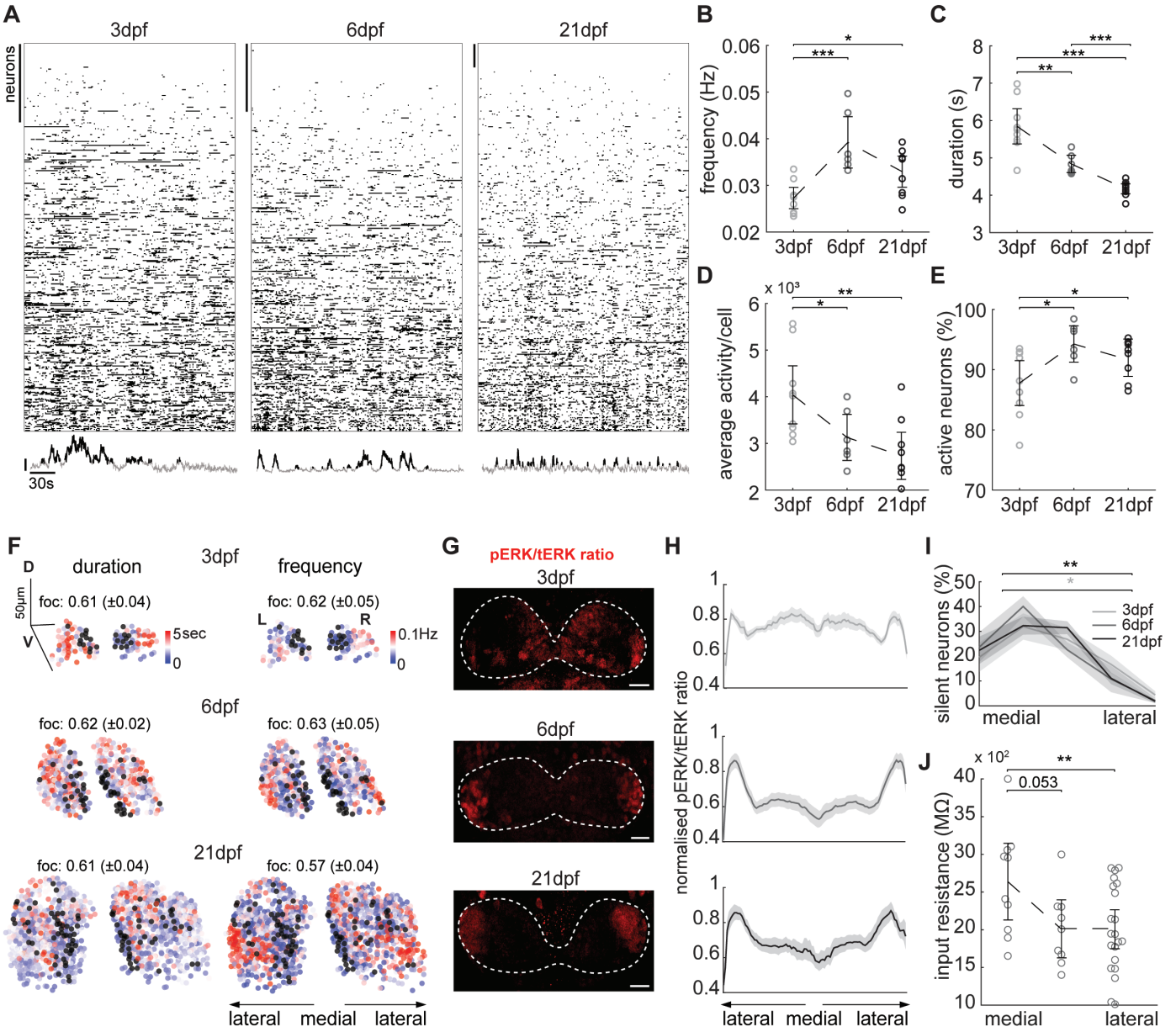

Figure 6: Features of habenular spontaneous activity change during development

(A) Individual spontaneous activity bursts (black markings) detected in all habenular neurons at 3,6 and 21dpf sorted based on their increasing overall activity rate. Black bars represent 100 neurons. Bottom panel shows individual example spontaneous activity traces from three different neurons, with detected events marked with black colour. Black bar represents 10% ΔF/F. (B) Average frequency of spontaneous activity bursts in habenular neurons in each zebrafish at 3dpf (n=9 fish), 6dpf (n=6 fish) and 21dpf (n=9 fish). (C) Average duration of spontaneous activity bursts in habenular neurons in each zebrafish. (D) Average spontaneous activity in habenular neurons in each zebrafish, represented as total area under the curve of all detected events. (E) The ratio of spontaneously active neurons with at least one spontaneous activity burst.*p<0.05, **p<0.01, ***p<0.001,Wilcoxon ranksum test. (F) Three-dimensional reconstructions of habenular neurons based on the duration (left) and frequency of their spontaneous activity events. Frequency and duration are colour coded. Black dots are inactive neurons. Coronal view. Scale bars represent 50µm. 'foc' represents the focality index as mean ±SEM for the temporal features of spontaneous activity bursts, duration and frequency, across all zebrafish and is depicted on top of the individual example's three-dimensional reconstruction. (G) Confocal microscopy images of pERK/tERK ratio in representative examples of habenula at 3,6 and 21dpf in dorsal view. White bar represents 20µm. White dashed lines delineate the borders of habenula. Note the difference in pERK/tERK ratio between medial and lateral ends of habenula. (H) Quantifications of the normalised pERK/tERK ratio along the mediolateral axis for each age at 3dpf (n=15), 6dpf (n=17) and 21dpf (n=8). Shading represents SEM. (I) The ratio of silent neurons in relation to their normalized mediolateral location along both habenula hemispheres of 3,6 and 21dpf. Shading represent SEM. Averages of the two most medial and two most lateral location bins were compared within one age. *p<0.05 for 3dpf, **p<0.01 for 21dpf, Wilcoxon signed-rank test. (J) Input resistance measured by intracellular recordings of habenular neurons (n=40) across the mediolateral axis of juvenile zebrafish. Medial neurons (n=10), central neurons (n=9) and lateral neurons (n=21) in 14 fish. **p<0.01, Wilcoxon ranksum test.
All data presented as mean ±SEM.

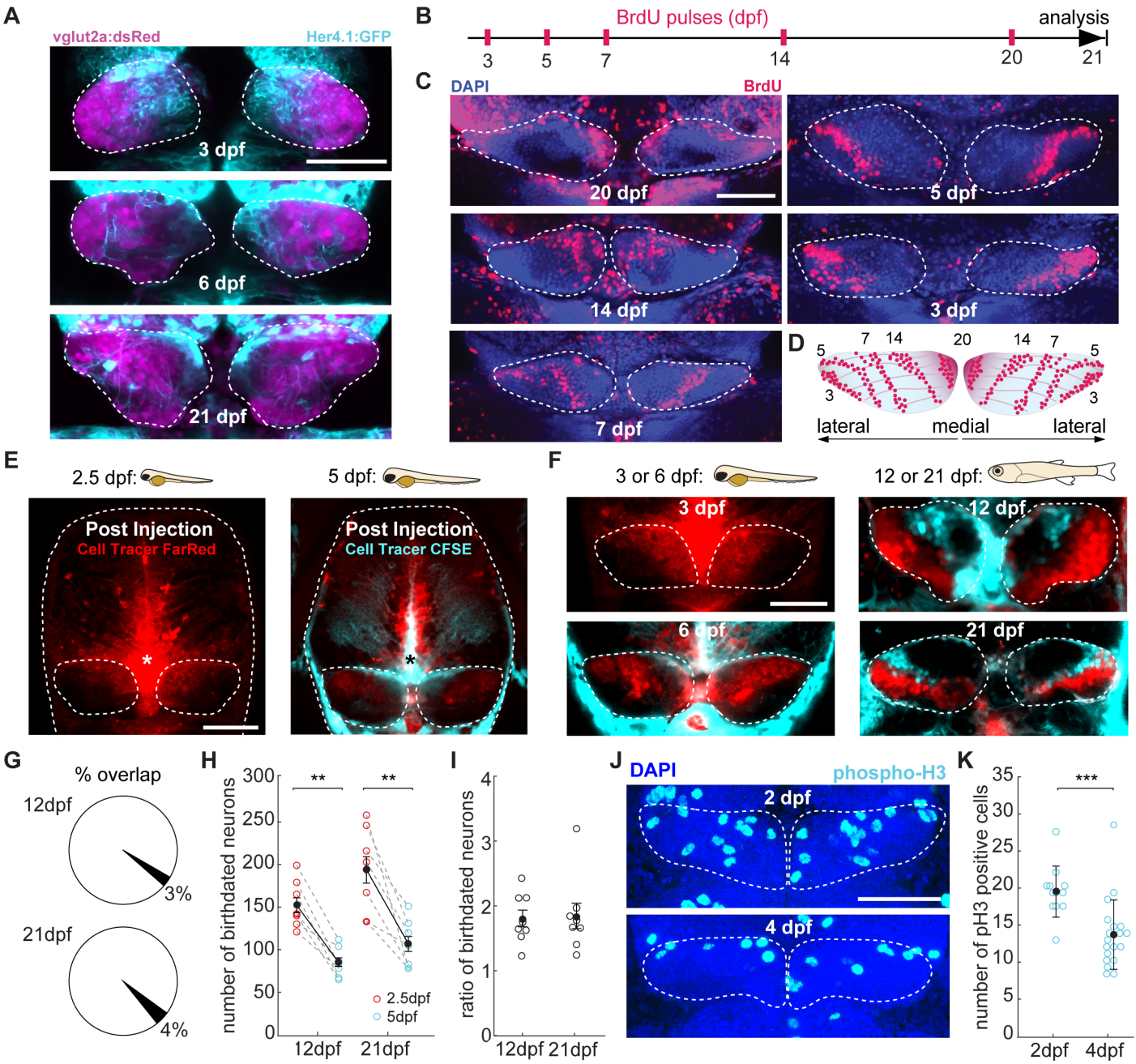

Figure 7: Distinct spatial domains of habenular neurons are born through sequential neurogenesis

(A) Confocal microscopy images of habenula in Tg(vglut2a:dsRed) and Tg(Her4:GFP) double transgenic zebrafish at 3, 6 and 21dpf, displaying the glutamatergic neurons (magenta) and potential neuronal progenitors of habenula labelled by Her4 expression (cyan), dorsal view. Bar represents 50µm. White dashed lines delineate the borders of habenula. (B) Schematic representation of BrdU pulse labelling protocol at 3, 5, 7, 14 and 20dpf. Animals were raised to 21dpf before imaging. (C) Confocal microscopy images of 21 dpf habenula (white dashed line) showing distribution of neurons that are born at different developmental stages. Neurons were birthdated by using BrdU (red) pulse labelling, at the developmental stages indicated in each panel. DAPI label marks all cells in blue. Dorsal view. Bar represents 50µm. (D) Schematic representation of the sequential arrangement of neurons that are born at different developmental stages along the mediolateral axis, dorsal view. (E) Confocal microscopy images of telencephalic ventricle 15 hours post injection with Cell Tracer FarRed (red) at 2,5dpf (left) and a second injection with Cell TracerCellTracer CFSE (cyan) at 5dpf (right). Dorsal view. Asterix shows injection site in the telencephalic ventricle. Borders of the zebrafish telencephalon and habenula are delineated by a dashed white line. Bar represents 50µm. (F) Confocal microscopy images of habenula one day post-injection of Cell Tracer FarRed (red) injected at 2,5dpf and CellTracer CFSE (cyan) injected at 5dpf (left panels). Birthdated habenular neurons are located near the medial wall of the habenula. At 12 and 21dpf (right panels), habenular neurons labelled at 2,5 and 5dpf exhibit distinct spatial distributions. Borders of the habenula are delineated by a dashed white line. Bar represents 50µm. (G) The ratio of overlap between the two populations of habenular neurons birthdated by the sequential injections of FarRed and CFSE cell tracers at 2,5 and 5dpf, respectively and quantified at 12dpf (n=8) and 21dpf (n=8). (H) The number of habenular neurons that were born at 2,5dpf vs 5dpf, measured at 12dpf (n=8) and 21dpf (n=8). **$p<0.01$, Wilcoxon ranksum test. (I) The ratio of habenular neurons birthdated at 2,5 vs 5dpf quantified at 12dpf (n=8) and 21dpf (n=8). (J) Confocal microscopy images of habenula labelled with phospho-H3 antibody (cyan) indicating mitotic cells at 2 and 4 dpf. DAPI label marks all cells in blue. Borders of the habenula are delineated by a dashed white line. Bar represents 50µm. (K) The number of phosphoH3 positive mitotic cells in the habenula, at 2 and 4 dpf. ***$p<0.001$, Wilcoxon ranksum test.

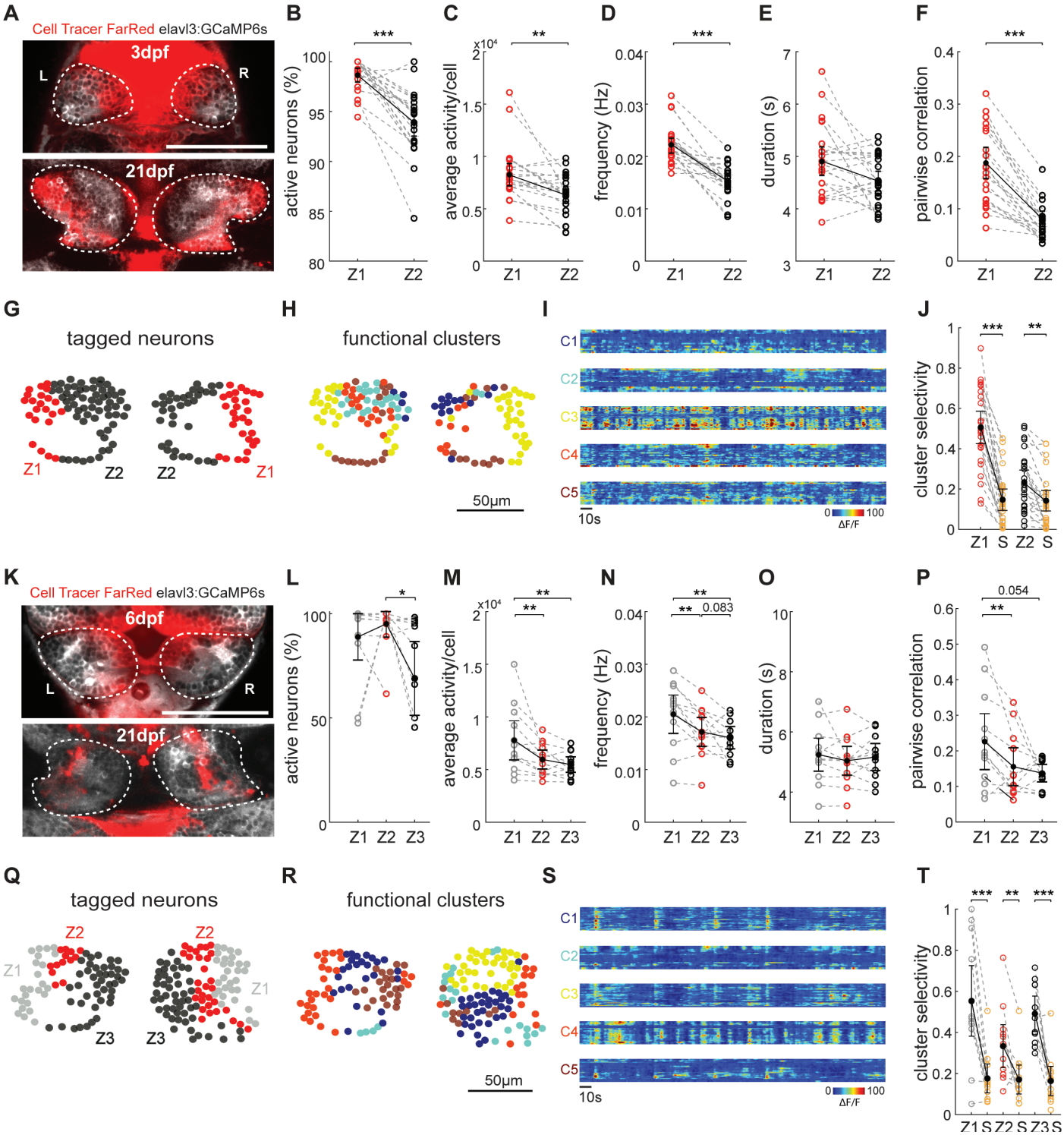

Figure 8: Habenular neurons that are born at a distinct developmental stage exhibit similar functional properties.
(A) Confocal microscopy images of elavl3:GCaMP6s (white) zebrafish habenula at 3 (top) and 21 (bottom) dpf, after the injection of the cell tracer Far Red (red) at 2,5 dpf. Dorsal view. Habenula is delineated by a dashed white line. Developmentally tagged, red-labelled neurons at 21dpf are in zone 1 (Z1= early born), whereas unlabelled neurons are in zone 2 (Z2= later born). Bars represent 100µm. L,left; R;right. (B) The ratio of spontaneously active Z1(red) vs Z2(black) habenular neurons at 21 dpf. Note that a higher ratio of early born habenular neurons in Z1 are active, when compared to later born neurons in Z2 (n=21 planes in 12 fish). (C) Average spontaneous activity that is represented as total area under the curve of all detected events, in Z1 vs Z2 habenular neurons at 21 dpf. (D) Average spontaneous activity burst frequency in Z1 vs Z2 habenular neurons at 21 dpf. (E) Average spontaneous activity burst duration in Z1 vs Z2 habenular neurons at 21 dpf. (F) Average pairwise correlations of Z1 vs Z2 habenular neurons at 21 dpf. Note that Z1 neurons are significantly more correlated than Z2 habenular neurons. **p<0.01, ***p<0.001, Wilcoxon signed-rank test. (G) Spatial distribution of labelled early born (Z1) vs later born (Z2) habenular neurons, in an example zebrafish at 21 dpf. (H) Spatial distribution of habenular neurons colour coded according to their functional clusters based on their spontaneous activity, using k-means clustering in the same example zebrafish as in I. (I) Colour coded neural traces showing the spontaneous activity of each habenular neuron that belong to a given cluster "C", in the same example zebrafish as G and H. Warm colours represents increased neural activity. Note the prominent overlap between the functional cluster C3 (yellow neurons in H) and Z1 neurons in G. (J) Cluster selectivity of Z1 vs Z2 habenular neurons, when compared to the same number of randomly selected habenular neurons

(Figure 7E). We raised the zebrafish larvae injected with cell tracers of two different colours (far-red, green) until 12 and 21dpf, and visualized the cohorts of birthdated habenular neurons in living juvenile zebrafish (Figure 7F). Our results revealed a distinct spatial organization of habenular neurons birthdated at 2,5dpf, compared to the neurons birthdated at 5dpf (Figure 7F). Furthermore, we observed less than 4% overlap of birthdated neurons by injections at 2,5 vs 5 dpf, highlighting the temporal resolution of our in vivo birthdating method (Figure 7G). Additionally, these experiments also revealed that the number of neurons birthdated at 2,5 dpf was almost double the number of neurons birthdated at 5 dpf (Figure 7H-I). This higher rate of habenular neurogenesis at earlier developmental stages is also in line with our observation for larger number of phosho-histone3 [103] labelled mitotic cells in habenula at earlier developmental stages (Figure 7J-K). Altogether, our results revealed that sequential neurogenesis in habenula generates spatially organized, non-overlapping clusters of habenular neurons.

Habenular neurons born at a distinct developmental stage, form a distinct functional cluster.

Our results in previous sections indicate a potential relationship between the birthdate of habenular neurons, spatial location and their functional properties. Based on these results, we hypothesized that the habenular neurons that are born together might form distinct functional clusters in habenula, with similar features of spontaneous activity. To test this hypothesis, we injected a far-red fluorescence cell tracer to the forebrain ventricles of zebrafish larvae expressing GCaMP6s at either 2,5 or 5dpf (Figure 8A,K). Later, we raised these animals to 21dpf and visualized their habenular activity in the green spectrum, while identifying birthdated habenular neurons in the far-red spectrum, by using confocal microscopy (Figure 8A,K). Our in vivo birthdating injections at 2,5 or 5dpf allowed us to classify habenular neurons into distinct spatial zones (Zs), where Z1 represents the earliest born (oldest) neurons and Z2, Z3 represents later born neurons with descending order of maturity (Z1>Z2>Z3) (figure 8G-Q).

Our analysis revealed striking differences in the functional features of the spontaneous activity between habenular neurons born at different developmental stages, corresponding to distinct spatial zones. Earlier born habenular neurons displayed stronger spontaneous activity (Figure 8B,C,L,M) with higher frequency (Figure 8D-N) and duration (Figure 8E). Moreover, earlier born habenular neurons showed a significantly larger number of pairwise correlations, compared to later born habenular neurons (Figure 8F,P). Our results suggest that distinct functional clusters of habenular neurons with distinct functional features are born at different developmental stages. To test this idea further, we asked whether the developmentally tagged neurons are also related to the spatially organized functional clusters within habenula, observed earlier (Figure 4A-D) [81]. To this end, we clustered the spontaneous habenular activity using k-means clustering (Figure 8H,I,R,S) and calculated the overlap between developmentally tagged neurons and functional clusters, using a 'cluster selectivity' index [81]. If developmentally tagged neurons in different habenular zones overlap with one functional cluster, "clusters selectivity" would result in 1. We observed that the developmentally tagged habenular neurons in each zone overlap with significantly fewer clusters, when compared to the same number of randomly selected habenular neurons (Figure 8J-T). These results revealed that distinct functional clusters of spatially organized habenular neurons are born at distinct developmental stages, and exhibit similar features of spontaneous activity.

Continuation legend figure 8:

(S) in yellow. Note that both Z1 and Z2 habenular neurons belong to fewer functional clusters compared to an equal number of random neurons. ***p<0.001, Wilcoxon signed-rank test. Also, note that Z1 neurons are significantly more cluster selective than Z2. ***p<0.001, Wilcoxon ranksum test. (K) Confocal microscopy images of elavl3:GCaMP6s (white) zebrafish habenula at 5 (top) and 21 (bottom) dpf, after the injection of the cell tracer (red) at 5 dpf. Oldest neurons (Z1= early born) are located lateral to the red-labelled neurons (Z2= intermediate born) that are developmentally tagged at 5dpf. The youngest neurons (Z3= late born) are located medial to the red-labelled neurons. Bars represent 100μm. L,left; R;right. (L) The ratio of spontaneously active Z1(gray), Z2(red), Z3 (black) habenular neurons at 21 dpf (n=12 planes in 5 fish). Note that a higher ratio of Z2 neurons are active, when compared to Z3 neurons. (M) Average spontaneous activity that is represented as total area under the curve of all detected events, in Z1, Z2, Z3 habenular neurons at 21 dpf. (N) Average spontaneous activity burst frequency in Z1, Z2, Z3 habenular neurons at 21 dpf. (O) Average spontaneous activity burst duration in Z1, Z2, Z3 habenular neurons at 21 dpf. (P) Average pairwise correlations of Z1, Z2, Z3 habenular neurons at 21 dpf.**p<0.01, ***p<0.001, Wilcoxon signed-rank test. (Q) Spatial distribution of early born (Z1), intermediate born (Z2), and later born (Z3) habenular neurons, in an example zebrafish at 21 dpf. (R) Spatial distribution of habenular neurons colour coded according to their functional clusters based on their spontaneous activity, using k-means clustering in the same example zebrafish as in I. (S) Colour coded neural traces showing the spontaneous activity of each habenular neuron that belong to a given cluster "C", in the same example zebrafish as G and H. Warm colours represents increased neural activity. (T) Cluster selectivity of Z1, Z2, Z3 habenular neurons, when compared to same number of randomly selected habenular neurons (S) in yellow. Note that Z1, Z2 and Z3 habenular neurons belong to fewer functional clusters compared to equal number of random neurons. ***p<0.001, Wilcoxon signed-rank test All data presented as mean ±SEM.

DISCUSSION

In this study, we investigated the functional development of habenular circuits in zebrafish across development from young larvae with relatively simple behaviours to juvenile zebrafish with complex behaviours [5-9, 79, 82, 83]. The use of juvenile zebrafish is gaining popularity due to their transparent brains and their expanded behavioural repertoire that requires habenular function [5-9, 83]. Our results revealed that as the zebrafish develop from the larval to the juvenile stage, habenular circuits undergo multiple transitions in its architecture, sensory computations, and intrinsically generated spontaneous activity, which could support the expansion of the behavioural repertoire during development.

Previous studies indicate the presence of olfactory [64, 80, 81] and visual [52, 53, 80] responses in habenula, which were suggested to be involved in generating odour avoidance [64], light preference [53] and circadian behaviours [65]. Both visual[104] and olfactory[105] responses are reported in sensory organs of 2,5 days old zebrafish larvae. However, the precise developmental maturation of these sensory inputs in habenula has not been investigated. Our results revealed that at early developmental stages habenula is first innervated by the visual inputs, which are followed by the olfactory inputs. This is also in line with our observation of light responses dominating habenula of larval zebrafish followed by olfactory responses for both aversive and attractive odours. Interestingly, we observed that other aversive stimuli, such as mechanical vibrations [1] and mild-electric stimulation [63, 73, 83], elicit responses in habenula only during later developmental stages. This gradual increase in stimulus diversity of habenular responses likely reflects a developmental transition of habenula into a multi-sensory processing brain region, which can encode stimuli with diverse hedonic valances. Remarkably, we observed that visual, olfactory and aversive information are distinctly encoded by the activation of separate neural populations. Such distinct encoding of different sensory modalities at all developmental stages highlights the important role of habenula in integrating information from multiple sensory systems [52, 53, 64, 80, 81].

As in other lower vertebrates [106], zebrafish dHb exhibits prominent molecular [70-73] and structural asymmetries [86]. Not surprisingly, habenular lateralization has important consequences with respect to the segregation of different sensory modalities across habenular hemispheres and for regulating the targeting of habenular axons to different output regions [63, 79, 86]. We observed that the functional lateralization of sensory inputs and computations in habenula is prominent mostly in the dHb, which develops early during development [85]. Whereas, we did not observe functional lateralization in vHb, which develops later [78, 84], despite the prominent sensory evoked vHb responses. This developmental order eventually leads to a decrease in functional lateralization across the entire habenula as the animals maturate. Interestingly, similar to primary sensory systems [26, 33, 107], maturation of zebrafish habenula requires the early presence of sensory inputs [80]. When these inputs are removed before a critical time window, zebrafish dHb loses its functional lateralization [80]. It is also important to note that aversive stimuli (mechanical vibrations and mild-electric stimulation) did not elicit lateralized responses in zebrafish habenula, which is in line with studies performed in the mammalian lateral habenula [55, 57, 59], where aversive responses showed no apparent lateralization [69]. We suggest that the apparent lack of lateralization in the mammalian habenula is due to a continued maturation of lateral habenula dominated by aversive cue responses and reduced availability of sensory information during mammalian in utero development.

The activity-dependent maturation of neural circuits does not solely rely on sensory inputs but also includes endogenously generated spontaneous activity [25]. In several brain regions spontaneously generated activity is thought to play important roles in the maturation of synaptic connections, refining network topography [30, 31, 39] and entraining developing circuits [43, 108, 109]. In our study, we observed that habenular networks exhibit spatially organized spontaneous activity already at early developmental stages. In fact, a recent transcriptomics study revealed a topographic organization of habenular neurons based on their distinct molecular features already in 10 days old zebrafish larvae [73], and likely overlap with the spatially organized spontaneous activity studied here. Whether the spontaneous activity is needed for the proper development of distinct habenular clusters or habenular function, as in other brain regions [30, 110] is yet to be investigated.

Interestingly, we also observed that temporal features of habenular spontaneous activity changed, leading to faster kinetics at older ages. The trend for faster kinetics of intrinsically generated activity across development was also observed in other higher brain regions, such as the hippocampus [40, 94]. What may underlie the faster kinetics of spontaneous activity bursts in older ages? It is likely that multiple processes can modulate spontaneous habenular activity leading to the observed dynamical changes during development. One possibility is that early spontaneous activity might be driven by glia [49] or other support cells [50], which usually generate slow bursts of activity. In fact, it was previously shown that astrocytes can modulate the bursting activity in the rodent habenula [111] and astroglia activation in zebrafish can excite nearby neurons [112]. Alternatively, it is possible that as the habenula

develops, synaptic connections between habenular neurons become more mature. Together with the increased inhibition we observed in the habenula, by the addition of GABAergic connections, such mature synapses can support faster neural dynamics. Finally, part of the habenular spontaneous activity might also be driven by the activation of the ancestral cortico-limbic homologs in the zebrafish forebrain. For example, it was shown that habenula is strongly driven by inputs received from entopeduncular nucleus [54, 62, 113] lateral hypothalamus [59] and cortex [55]. Hence it is likely that the homologues of these input regions are not yet fully developed and cannot drive habenular activity in young zebrafish larvae. A recent study showed that zebrafish equivalent of amygdala (Dm) [114], driving both entopeduncular nucleus and lateral hypothalamus [114], also develop during late juvenile stage [115]. Taken together, we suggest that all these processes jointly contribute to the habenular spontaneous activity.

Our results revealed that the developmental changes in the temporal kinetics of habenular spontaneous activity are accompanied by the sequential addition of newborn neurons across development. More specifically, we found that the spatially confined locations of neuronal clusters that are born during distinct developmental stages, follow a mediolateral arrangement. In this arrangement, youngest neurons are located closer to the neural progenitors of the habenula on the medial wall, while the oldest habenular neurons are located closer to the lateral wall. Similar sequential stacking of newly born neurons was also observed during forebrain development in both zebrafish [116] and rodents [15-17]. Moreover, such a sequential order of neurogenesis contributes to different neural subtypes in the zebrafish hindbrain and spinal cord [21-24], as well as the rodent entorhinal cortex [12]. Hence it is possible that recently described populations of habenular neurons with distinct molecular identities [73] might be born during different developmental stages of the zebrafish habenula. The topographically organized molecular [73] and functional clusters [73, 81, 83] of habenular neurons represent the distinct subdomains or functional modules of habenula and are likely associated with different aspects of animal behaviour. Our data revealed that at least two of the functional clusters within habenula are born at two different developmental stages, stay in spatially confined locations and exhibit different functional features. Therefore, we propose that the distinct functional clusters of habenular neurons are born at different developmental time points. In turn, such a developmental order could contribute to an increased diversity of habenular neurons and expand habenular function across development. These ideas are in line with several recent studies that suggest that complex and cognitively demanding behaviours arise later in development as animals maturate [5-7, 79, 83]. Our findings in habenula suggest that such expansion of animal behaviour might be due to the incorporation of new functional modules at different developmental time points. In the future, it will be interesting to see whether such sequential addition of new neuronal modules with distinct functional properties is a feature that is not only unique to habenula but is also preserved across the brain.

ACKNOWLEDGEMENTS

We thank M. Ahrens (HHMI, Janelia Farm, USA), C. Wyart (ICM, Paris, France), H. Baier (MPI, Martinsried, Germany) and Shin-ichi Higashijima (Okazaki Institute for Integrative Bioscience, Japan) for transgenic lines. We thank S. Eggen, M. Andresen, V. Nguyen and our fish facility support team for technical assistance. We thank the Yaksi lab members for stimulating discussions. This work was funded by ERC starting grant 335561 (S.F., E.Y.), Helse Midt-Norge Samarbeidsorganet grant (N.J.-Y. and E.Y.), RCN FRIPRO Research Grant 239973 (E.Y.), Boehringer Ingelheim Fonds (C.R). Work in the E.Y. lab is funded by the Kavli Institute for Systems Neuroscience at NTNU.

AUTHOR CONTRIBUTIONS

Conceptualization, S.F., E.Y.; Methodology and data, S.F., F.A-H., K.A.M., E.M.B.K., B.S., N.G.F., K.T.P.C., M.I.C., N.J.Y., C.K.; Data Analysis, S.F., F.A-H ., K.A.M., E.M.B.K., B.S., N.G.F., K.T.P.C., C.D.V., F.P., C.R., N.J.Y.; Investigation, all authors; Writing, S.F., F.A-H ., E.Y.; Review & Editing, all authors; Funding Acquisition and Supervision, E.Y.

DECLARATION OF INTERESTS

The authors declare that they have no competing interests

REFERENCES

1. Burgess, H.A. and M. Granato, Sensorimotor gating in larval zebrafish. J Neurosci, 2007. 27(18): p. 4984-94.
2. Heap, L.A.L., et al., Luminance Changes Drive Directional Startle through a Thalamic Pathway. Neuron, 2018. 99(2): p. 293-301 e4.
3. Temizer, I., et al., A Visual Pathway for Looming-Evoked Escape in Larval Zebrafish. Curr Biol, 2015. 25(14): p. 1823-34.
4. Lindsay, S.M. and R.G. Vogt, Behavioral responses of newly hatched zebrafish (Danio rerio) to amino acid chemostimulants. Chem Senses, 2004. 29(2): p. 93-100.
5. Valente, A., et al., Ontogeny of classical and operant learning behaviors in zebrafish. Learn Mem, 2012. 19(4): p. 170-7.

6. Yashina, K., et al., Zebrafish Exploit Visual Cues and Geometric Relationships to Form a Spatial Memory. iScience, 2019. 19: p. 119-134.
7. Palumbo, F., et al., The zebrafish dorsolateral habenula is required for updating learned behaviors. bioRxiv, 2020: p. 802256.
8. Dreosti, E., et al., Development of social behavior in young zebrafish. Front Neural Circuits, 2015. 9: p. 39.
9. Hinz, R.C. and G.G. de Polavieja, Ontogeny of collective behavior reveals a simple attraction rule. Proc Natl Acad Sci U S A, 2017. 114(9): p. 2295-2300.
10. Brenowitz, E.A. and M.D. Beecher, Song learning in birds: diversity and plasticity, opportunities and challenges. Trends Neurosci, 2005. 28(3): p. 127-32.
11. Anderson, J.R., The development of self-recognition: a review. Dev Psychobiol, 1984. 17(1): p. 35-49.
12. Donato, F., et al., Stellate cells drive maturation of the entorhinal-hippocampal circuit. Science, 2017. 355(6330).
13. Bjerknes, T.L., et al., Path integration in place cells of developing rats. Proc Natl Acad Sci U S A, 2018. 115(7): p. E1637-E1646.
14. Tottenham, N. and L.J. Gabard-Durnam, The developing amygdala: a student of the world and a teacher of the cortex. Curr Opin Psychol, 2017. 17: p. 55-60.
15. Angevine, J.B., Jr. and R.L. Sidman, Autoradiographic study of cell migration during histogenesis of cerebral cortex in the mouse. Nature, 1961. 192: p. 766-8.
16. Luskin, M.B. and C.J. Shatz, Neurogenesis of the cat's primary visual cortex. J Comp Neurol, 1985. 242(4): p. 611-31.
17. Lein, E.S., et al., Transcriptomic Perspectives on Neocortical Structure, Development, Evolution, and Disease. Annu Rev Neurosci, 2017. 40: p. 629-652.
18. Sur, M. and C.A. Leamey, Development and plasticity of cortical areas and networks. Nat Rev Neurosci, 2001. 2(4): p. 251-62.
19. Jabaudon, D., Fate and freedom in developing neocortical circuits. Nat Commun, 2017. 8: p. 16042.
20. Mayer, S., et al., Multimodal Single-Cell Analysis Reveals Physiological Maturation in the Developing Human Neocortex. Neuron, 2019. 102(1): p. 143-158 e7.
21. Koyama, M., et al., Mapping a sensory-motor network onto a structural and functional ground plan in the hindbrain. Proc Natl Acad Sci U S A, 2011. 108(3): p. 1170-5.
22. Pujala, A. and M. Koyama, Chronology-based architecture of descending circuits that underlie the development of locomotor repertoire after birth. Elife, 2019. 8.
23. McLean, D.L. and J.R. Fetcho, Ontogeny and innervation patterns of dopaminergic, noradrenergic, and serotonergic neurons in larval zebrafish. J Comp Neurol, 2004. 480(1): p. 38-56.
24. McLean, D.L. and J.R. Fetcho, Spinal interneurons differentiate sequentially from those driving the fastest swimming movements in larval zebrafish to those driving the slowest ones. J Neurosci, 2009. 29(43): p. 13566-77.
25. Penn, A.A. and C.J. Shatz, Brain waves and brain wiring: the role of endogenous and sensory-driven neural activity in development. Pediatr Res, 1999. 45(4 Pt 1): p. 447-58.
26. Wiesel, T.N. and D.H. Hubel, Comparison of the effects of unilateral and bilateral eye closure on cortical unit responses in kittens. J Neurophysiol, 1965. 28(6): p. 1029-40.
27. Yuste, R., Introduction: spontaneous activity in the developing central nervous system. Semin Cell Dev Biol, 1997. 8(1): p. 1-4.
28. O'Donovan, M.J., Motor activity in the isolated spinal cord of the chick embryo: synaptic drive and firing pattern of single motoneurons. J Neurosci, 1989. 9(3): p. 943-58.
29. Galli, L. and L. Maffei, Spontaneous impulse activity of rat retinal ganglion cells in prenatal life. Science, 1988. 242(4875): p. 90-1.
30. Moreno-Juan, V., et al., Prenatal thalamic waves regulate cortical area size prior to sensory processing. Nat Commun, 2017. 8: p. 14172.
31. Katz, L.C. and C.J. Shatz, Synaptic activity and the construction of cortical circuits. Science, 1996. 274(5290): p. 1133-8.
32. White, L.E., D.M. Coppola, and D. Fitzpatrick, The contribution of sensory experience to the maturation of orientation selectivity in ferret visual cortex. Nature, 2001. 411(6841): p. 1049-52.
33. Webster, D.B. and M. Webster, Neonatal sound deprivation affects brain stem auditory nuclei. Arch Otolaryngol, 1977. 103(7): p. 392-6.
34. Zou, D.J., et al., Postnatal refinement of peripheral olfactory projections. Science, 2004. 304(5679): p. 1976-9.
35. Maffei, L. and L. Galli-Resta, Correlation in the discharges of neighboring rat retinal ganglion cells during prenatal life. Proc Natl Acad Sci U S A, 1990. 87(7): p. 2861-4.
36. Ben-Ari, Y., Developing networks play a similar melody. Trends Neurosci, 2001. 24(6): p. 353-60.
37. Elstrott, J., et al., Direction selectivity in the retina is established independent of visual experience and cholinergic retinal waves. Neuron, 2008. 58(4): p. 499-506.
38. Feller, M.B., Spontaneous correlated activity in developing neural circuits. Neuron, 1999. 22(4): p. 653-6.
39. Xu, H.P., et al., An instructive role for patterned spontaneous retinal activity in mouse visual map development. Neuron, 2011. 70(6): p. 1115-27.
40. Leinekugel, X., et al., Giant depolarizing potentials: the septal pole of the hippocampus paces the activity of the developing intact septohippocampal complex in vitro. J Neurosci, 1998. 18(16): p. 6349-57.
41. Rudy, J.W., S. Stadler-Morris, and P. Albert, Ontogeny of spatial navigation behaviors in the rat: dissociation of "proximal"- and "distal"-cue-based behaviors. Behav Neurosci, 1987. 101(1): p. 62-73.
42. Altman, J., R.L. Brunner, and S.A. Bayer, The hippocampus and behavioral maturation. Behav Biol, 1973. 8(5): p. 557-96.
43. Gretenkord, S., et al., Coordinated electrical activity in the olfactory bulb gates the oscillatory entrainment of entorhinal networks in neonatal mice. PLoS Biol, 2019. 17(1): p. e2006994.
44. Yu, Y.C., et al., Preferential electrical coupling regulates neocortical lineage-dependent microcircuit assembly. Nature, 2012. 486(7401): p. 113-7.

45. Kerschensteiner, D., Spontaneous Network Activity and Synaptic Development. Neuroscientist, 2014. 20(3): p. 272-90.
46. Meister, M., et al., Synchronous bursts of action potentials in ganglion cells of the developing mammalian retina. Science, 1991. 252(5008): p. 939-43.
47. O'Donovan, M.J., N. Chub, and P. Wenner, Mechanisms of spontaneous activity in developing spinal networks. J Neurobiol, 1998. 37(1): p. 131-45.
48. Yuste, R., A. Peinado, and L.C. Katz, Neuronal domains in developing neocortex. Science, 1992. 257(5070): p. 665-9.
49. Zhang, R.W., et al., Muller Glial Cells Participate in Retinal Waves via Glutamate Transporters and AMPA Receptors. Cell Rep, 2019. 27(10): p. 2871-2880 e2.
50. Babola, T.A., et al., Homeostatic Control of Spontaneous Activity in the Developing Auditory System. Neuron, 2018. 99(3): p. 511-524 e5.
51. Miyasaka, N., et al., From the olfactory bulb to higher brain centers: genetic visualization of secondary olfactory pathways in zebrafish. J Neurosci, 2009. 29(15): p. 4756-67.
52. Cheng, R.K., et al., Characterization of a thalamic nucleus mediating habenula responses to changes in ambient illumination. BMC Biol, 2017. 15(1): p. 104.
53. Zhang, B.B., et al., Left Habenula Mediates Light-Preference Behavior in Zebrafish via an Asymmetrical Visual Pathway. Neuron, 2017. 93(4): p. 914-928 e4.
54. Turner, K.J., et al., Afferent Connectivity of the Zebrafish Habenulae. Front Neural Circuits, 2016. 10: p. 30.
55. Warden, M.R., et al., A prefrontal cortex-brainstem neuronal projection that controls response to behavioural challenge. Nature, 2012. 492(7429): p. 428-32.
56. Okamoto, H., M. Agetsuma, and H. Aizawa, Genetic dissection of the zebrafish habenula, a possible switching board for selection of behavioral strategy to cope with fear and anxiety. Dev Neurobiol, 2012. 72(3): p. 386-94.
57. Matsumoto, M. and O. Hikosaka, Lateral habenula as a source of negative reward signals in dopamine neurons. Nature, 2007. 447(7148): p. 1111-5.
58. Meye, F.J., et al., Shifted pallidal co-release of GABA and glutamate in habenula drives cocaine withdrawal and relapse. Nat Neurosci, 2016. 19(8): p. 1019-24.
59. Lazaridis, I., et al., A hypothalamus-habenula circuit controls aversion. Mol Psychiatry, 2019.
60. Stamatakis, A.M., et al., A unique population of ventral tegmental area neurons inhibits the lateral habenula to promote reward. Neuron, 2013. 80(4): p. 1039-53.
61. Hong, S., et al., Negative reward signals from the lateral habenula to dopamine neurons are mediated by rostromedial tegmental nucleus in primates. J Neurosci, 2011. 31(32): p. 11457-71.
62. Herkenham, M. and W.J. Nauta, Afferent connections of the habenular nuclei in the rat. A horseradish peroxidase study, with a note on the fiber-of-passage problem. J Comp Neurol, 1977. 173(1): p. 123-46.
63. Duboue, E.R., et al., Left Habenular Activity Attenuates Fear Responses in Larval Zebrafish. Curr Biol, 2017. 27(14): p. 2154-2162 e3.
64. Krishnan, S., et al., The right dorsal habenula limits attraction to an odor in zebrafish. Curr Biol, 2014. 24(11): p. 1167-75.
65. Lin, Q. and S. Jesuthasan, Masking of a circadian behavior in larval zebrafish involves the thalamo-habenula pathway. Sci Rep, 2017. 7(1): p. 4104.
66. Hikosaka, O., The habenula: from stress evasion to value-based decision-making. Nat Rev Neurosci, 2010. 11(7): p. 503-13.
67. Flanigan, M., et al., An emerging role for the lateral habenula in aggressive behavior. Pharmacol Biochem Behav, 2017. 162: p. 79-86.
68. Yang, Y., et al., Ketamine blocks bursting in the lateral habenula to rapidly relieve depression. Nature, 2018. 554(7692): p. 317-322.
69. Huang, L., et al., A Visual Circuit Related to Habenula Underlies the Antidepressive Effects of Light Therapy. Neuron, 2019.
70. Aizawa, H., et al., Molecular characterization of the subnuclei in rat habenula. J Comp Neurol, 2012. 520(18): p. 4051-66.
71. deCarvalho, T.N., et al., Neurotransmitter map of the asymmetric dorsal habenular nuclei of zebrafish. Genesis, 2014. 52(6): p. 636-55.
72. Viswanath, H., et al., The medial habenula: still neglected. Front Hum Neurosci, 2013. 7: p. 931.
73. Pandey, S., et al., Comprehensive Identification and Spatial Mapping of Habenular Neuronal Types Using Single-Cell RNA-Seq. Curr Biol, 2018. 28(7): p. 1052-1065 e7.
74. Seigneur, E., J.S. Polepalli, and T.C. Sudhof, Cbln2 and Cbln4 are expressed in distinct medial habenula-interpeduncular projections and contribute to different behavioral outputs. Proc Natl Acad Sci U S A, 2018. 115(43): p. E10235-E10244.
75. Ren, J., et al., Habenula "cholinergic" neurons co-release glutamate and acetylcholine and activate postsynaptic neurons via distinct transmission modes. Neuron, 2011. 69(3): p. 445-52.
76. Agetsuma, M., et al., The habenula is crucial for experience-dependent modification of fear responses in zebrafish. Nat Neurosci, 2010. 13(11): p. 1354-6.
77. Lee, A., et al., The habenula prevents helpless behavior in larval zebrafish. Curr Biol, 2010. 20(24): p. 2211-6.
78. Amo, R., et al., Identification of the zebrafish ventral habenula as a homolog of the mammalian lateral habenula. J Neurosci, 2010. 30(4): p. 1566-74.
79. Amo, R., et al., The habenulo-raphe serotonergic circuit encodes an aversive expectation value essential for adaptive active avoidance of danger. Neuron, 2014. 84(5): p. 1034-48.
80. Dreosti, E., et al., Left-right asymmetry is required for the habenulae to respond to both visual and olfactory stimuli. Curr Biol, 2014. 24(4): p. 440-5.
81. Jetti, S.K., N. Vendrell-Llopis, and E. Yaksi, Spontaneous activity governs olfactory representations in spatially organized habenular microcircuits. Curr Biol, 2014. 24(4): p. 434-9.
82. Chou, M.Y., et al., Social conflict resolution regulated by

two dorsal habenular subregions in zebrafish. Science, 2016. 352(6281): p. 87-90.
83. Andalman, A.S., et al., Neuronal Dynamics Regulating Brain and Behavioral State Transitions. Cell, 2019. 177(4): p. 970-985 e20.
84. Beretta, C.A., et al., The ventral habenulae of zebrafish develop in prosomere 2 dependent on Tcf7l2 function. Neural Dev, 2013. 8: p. 19.
85. Aizawa, H., et al., Temporally regulated asymmetric neurogenesis causes left-right difference in the zebrafish habenular structures. Dev Cell, 2007. 12(1): p. 87-98.
86. Bianco, I.H., et al., Brain asymmetry is encoded at the level of axon terminal morphology. Neural Dev, 2008. 3: p. 9.
87. Ahumada-Galleguillos, P., et al., Directional asymmetry in the volume of the human habenula. Brain Struct Funct, 2017. 222(2): p. 1087-1092.
88. Hashikawa, Y., et al., Transcriptional and Spatial Resolution of Cell Types in the Mammalian Habenula. Neuron, 2020.
89. Vladimirov, N., et al., Light-sheet functional imaging in fictively behaving zebrafish. Nat Methods, 2014. 11(9): p. 883-4.
90. Satou, C., et al., Transgenic tools to characterize neuronal properties of discrete populations of zebrafish neurons. Development, 2013. 140(18): p. 3927-31.
91. Scott, E.K. and H. Baier, The cellular architecture of the larval zebrafish tectum, as revealed by gal4 enhancer trap lines. Front Neural Circuits, 2009. 3: p. 13.
92. Mohamed, G.A., et al., Optical inhibition of larval zebrafish behaviour with anion channelrhodopsins. BMC Biol, 2017. 15(1): p. 103.
93. Yaksi, E., B. Judkewitz, and R.W. Friedrich, Topological reorganization of odor representations in the olfactory bulb. PLoS Biol, 2007. 5(7): p. e178.
94. Buzsaki, G. and A. Draguhn, Neuronal oscillations in cortical networks. Science, 2004. 304(5679): p. 1926-9.
95. Romano, S.A., et al., An integrated calcium imaging processing toolbox for the analysis of neuronal population dynamics. PLoS Comput Biol, 2017. 13(6): p. e1005526.
96. Randlett, O., et al., Whole-brain activity mapping onto a zebrafish brain atlas. Nat Methods, 2015. 12(11): p. 1039-46.
97. Wee, C.L., et al., A bidirectional network for appetite control in larval zebrafish. Elife, 2019. 8.
98. Wee, C.L., et al., Zebrafish oxytocin neurons drive nocifensive behavior via brainstem premotor targets. Nat Neurosci, 2019. 22(9): p. 1477-1492.
99. Yeo, S.Y., et al., Fluorescent protein expression driven by her4 regulatory elements reveals the spatiotemporal pattern of Notch signaling in the nervous system of zebrafish embryos. Dev Biol, 2007. 301(2): p. 555-67.
100. Valiullina, F., et al., Developmental Changes in Electrophysiological Properties and a Transition from Electrical to Chemical Coupling between Excitatory Layer 4 Neurons in the Rat Barrel Cortex. Front Neural Circuits, 2016. 10: p. 1.
101. Govindan, S., P. Oberst, and D. Jabaudon, In vivo pulse labeling of isochronic cohorts of cells in the central nervous system using FlashTag. Nat Protoc, 2018. 13(10): p. 2297-2311.
102. Olstad, E.W., et al., Ciliary Beating Compartmentalizes Cerebrospinal Fluid Flow in the Brain and Regulates Ventricular Development. Curr Biol, 2019. 29(2): p. 229-241 e6.
103. Hendzel, M.J., et al., Mitosis-specific phosphorylation of histone H3 initiates primarily within pericentromeric heterochromatin during G2 and spreads in an ordered fashion coincident with mitotic chromosome condensation. Chromosoma, 1997. 106(6): p. 348-60.
104. Zhang, R.W., et al., Development of light response and GABAergic excitation-to-inhibition switch in zebrafish retinal ganglion cells. J Physiol, 2010. 588(Pt 14): p. 2557-69.
105. Bergboer, J.G.M., et al., Assaying sensory ciliopathies using calcium biosensor expression in zebrafish ciliated olfactory neurons. Cilia, 2018. 7: p. 2.
106. Concha, M.L. and S.W. Wilson, Asymmetry in the epithalamus of vertebrates. J Anat, 2001. 199(Pt 1-2): p. 63-84.
107. Moorman, S.J., et al., Stimulus dependence of the development of the zebrafish (Danio rerio) vestibular system. J Neurobiol, 1999. 38(2): p. 247-58.
108. Huberman, A.D., C.M. Speer, and B. Chapman, Spontaneous retinal activity mediates development of ocular dominance columns and binocular receptive fields in v1. Neuron, 2006. 52(2): p. 247-54.
109. Clause, A., et al., The precise temporal pattern of prehearing spontaneous activity is necessary for tonotopic map refinement. Neuron, 2014. 82(4): p. 822-35.
110. Anton-Bolanos, N., et al., Prenatal activity from thalamic neurons governs the emergence of functional cortical maps in mice. Science, 2019. 364(6444): p. 987-990.
111. Cui, Y., et al., Astroglial Kir4.1 in the lateral habenula drives neuronal bursts in depression. Nature, 2018. 554(7692): p. 323-327.
112. Diaz Verdugo, C., et al., Glia-neuron interactions underlie state transitions to generalized seizures. Nat Commun, 2019. 10(1): p. 3830.
113. Hong, S. and O. Hikosaka, The globus pallidus sends reward-related signals to the lateral habenula. Neuron, 2008. 60(4): p. 720-9.
114. Lal, P., et al., Identification of a neuronal population in the telencephalon essential for fear conditioning in zebrafish. BMC Biol, 2018. 16(1): p. 45.
115. von Trotha, J.W., P. Vernier, and L. Bally-Cuif, Emotions and motivated behavior converge on an amygdala-like structure in the zebrafish. Eur J Neurosci, 2014. 40(9): p. 3302-15.
116. Furlan, G., et al., Life-Long Neurogenic Activity of Individual Neural Stem Cells and Continuous Growth Establish an Outside-In Architecture in the Teleost Pallium. Curr Biol, 2017. 27(21): p. 3288-3301 e3.
117. Lister, J.A., et al., nacre encodes a zebrafish microphthalmia-related protein that regulates neural-crest-derived pigment cell fate. Development, 1999. 126(17): p. 3757-67.
118. Park, H.C., et al., Analysis of upstream elements in the HuC promoter leads to the establishment of transgenic zebrafish

with fluorescent neurons. Dev Biol, 2000. 227(2): p. 279-93.
119. Kermen, F., et al., Investigating olfactory behaviors in adult zebrafish. bioRxiv, 2019: p. 859033.
120. Kermen, F., et al., Interhemispheric connections between olfactory bulbs improve odor detection. PLoS Biol, 2020. 18(4): p. e3000701.
121. Reiten, I., et al., Motile-Cilia-Mediated Flow Improves Sensitivity and Temporal Resolution of Olfactory Computations. Curr Biol, 2017. 27(2): p. 166-174.
122. Bergen, J.R., et al. Hierarchical model-based motion estimation. 1992. Berlin, Heidelberg: Springer Berlin Heidelberg.
properties of discrete populations of zebrafish neurons. Development 140, 3927-3931.

MATERIAL AND METHODS

Contact for Reagent and Resource Sharing

Further information and requests for reagents may be directed to, and will be fulfilled by the lead author Emre Yaksi (emre.yaksi@ntnu.no).

Fish maintenance

The animal facilities and maintenance of zebrafish, Danio rerio, were approved by the Norwegian Food Safety Authority. Fish were kept in 3.5liter tanks at a density of 15-20 fish per tank in a Techniplast Zebtech Multilinking system at 28°C, pH 7, 6.0ppm O2 and 700μS, at a 14:10 hour light/dark cycle. Fish received a normal diet of dry food (Zebrafeed, Sparos) two times per day and Artemia nauplii once a day (Grade0, platinum Label, Argent Laboratories). Larvae were maintained in egg water (1.2g marine salt and 0.1% methylene blue in 20L RO water) from fertilization to 3dpf. From 3dpf to 6dpf larvae were kept in artificial fish water (AFW): 1.2g marine salt in 20L RO water. Animals used for experiments at 21dpf were transferred to 3.5 liter tanks in the zebrafish facility at 3dpf.

All experimental procedures performed on zebrafish larvae and juveniles were in accordance with the Directive 2010/63/EU of the European Parliament and the Council of the European Union and approved by the Norwegian Food Safety Authorities and Landesdirektion Sachsen, Germany (permit numbers TVV-52/2015 and TVV-35/2016).

For experiments the following fish lines were used: Tg(elavl3:GCaMP6s) [89], Tg(gad1b:GFP) [90], Tg(vglut2a:dsRed) [51], Tg(Lhx2a:gap-YFP) [51], Et(-0.6hsp70l:Gal4-VP16) s1020t; UAS:nfsB-mCherry [91], Tg(her4.1:GFP) [99]. Experiments were performed on embryos of nacre (mitfa[117]) background.

Confocal anatomical imaging

Prior to embedding, fish were anaesthetized with 0.02% MS222. Animals were then embedded in 1% (for 3-6dpf) or 2% (for 21dpf) low-melting-point agarose (LMP, Fisher Scientific) in a recording chamber (Fluorodish, World Precision Instruments) with AFW. Anatomical Z-scans were acquired using a Zeiss Examiner Z1 confocal microscope with a 20x water-immersion objective (Zeiss, NA 1.0, Plan-Apochromat) at room temperature, using 4-10x average for each plane.

BrDU labelling, immuno-staining and imaging

Labelling of newborn neurons with BrdU was performed at 3,5; 5,5; 7,5; 14,5; 20,5dpf in Tg(HuC:GFP) [118] fish outcrossed to wild type (AB) fish. 25-hpf embryos were dechorionated by Proteinase K (0.1 mg/ml) (Cat#:25530049) at room temperature and washed several times with 1x E3 medium. A stock of 10 mM BrdU (Sigma, Cat# B5002) in 1x E3 medium was prepared, aliquoted, and stored at -20 °C until use. For each treatment, a final concentration of 500 μM BrdU was applied to 3, and 5 dpf fish. For 7, 14 and 21 dpf fish, 2.5 mM BrdU was used. Treatments were all performed for 5 hours. Fish were kept in a dark incubator until 5 dpf and were transferred to the water system at 6 dpf. From this point on, 14/10 hours light/dark cycle was maintained. At 22 dpf, fish were sacrificed and fixed in 4% PFA-1% DMSO at +4 °C overnight, washed with 0.8% Triton-X in 1X PBS (PBSTx), dehydrated by a serial methanol gradient, and kept at -20 °C until further use. For immunohistochemical stainings, fish were rehydrated back to the aqueous phase (1X PBS). Brains were dissected out in cold 1x PBS and were incubated in pre-cooled acetone for 10 mins at -20°C. Brains were incubated in preheated 2mM HCl at 37 °C for 12 minutes, were cooled at room temperature for 10 min, and washed with 0.8% PBSTx. Samples were incubated in Rat anti-BrdU IgG (1:200 Bio-Rad, Cat# MCA2060) monoclonal antibody overnight at +4 °C. After serial washes in 0.8% PBSTx, the secondary antibody (Goat anti-rat Alexa 555, 1:500 dilution, ThermoFisher, Cat#A-21434) and DAPI at 1:3000 dilution were applied. Following an overnight incubation at +4 °C, samples were washed for a total of 2 hours with 0.8% PBSTx.

For measuring of pERK/tERK ratio, Fish were euthanized and fixed in cooled 4% PFA in 0.25% PBTx (0,25% Triton X-100 in 1X PBS) overnight (O/N) at 4°C. Samples were permeabilized in 0.50% Trypsin-EDTA on ice for 40min and washed. The samples were then incubated in the blocking solution (2% Normal Goat Serum, 1% BSA, 1% DMSO in 0.25% PBTx) for 1 hour followed by incubation in primary antibody solution (1:500 Ab, 1% BSA, 1% DMSO in 0.25% PBTx) overnight at 4°C. Next, samples were washed and incubated with secondary

antibody solution (1:1000 Ab, 1:1000 DAPI, 1% BSA, 1% DMSO in 0.25% PBTx) overnight at 4°C. Finally, samples were washed and placed in glycerol. pERK/tERK ratio of the median z-projection confocal images were calculated in ImageJ (Fiji). The pERK/tERK ratio is normalized by the maximum pERK/tERK ratio and adjusted for the habenular size using a custom-made script in Matlab.

For phospho-histone 3 staining, larvae were fixed in 4% PFA for 2h at room temperature or overnight at 4°C. Following washes in 0.3% Triton-X in PBS (0.3%PSBTx), fixed samples were permeabilized in 100% Acetone at -20°C for 20min, blocked in 0.3%PSBTx containing 0.1%BSA. Samples were incubated with the primary antibody (phospho-histone 3, Santa Cruz, #sc-8656-R, 1:500 dilution) overnight at +4 °C, followed by serial washes in 0.3%PSBTx, and incubation with the secondary antibody (goat anti-rabbit Alexa 488 plus, ThermoFisher, #A-11034, 1:1000 dilution) overnight at +4 °C. Next, samples were incubated in DAPI (1:1000) for 2h, before serial washes in 0.3%PSBTx.

For preservation, samples were transferred to 80% Glycerol in 1X PBS and were kept at +4 °C in the dark. For imaging, labelled brains were mounted in 80% glycerol on a glass slide with a cover slip. Anatomical Z-scans of habenula were acquired using a Zeiss Examiner Z1 confocal microscope with a 20x plan NA 0.8 objective, using 2-10x average for each plane. Phospho-histone3 positive cells were manually counted on confocal stack using the Cell Counter Plugin of Fiji/ImageJ.

In vivo two-photon calcium imaging and sensory stimulation

Two-photon calcium imaging was performed on 3dpf, 6dpf, and 21dpf old Tg(elavl3:GCaMP6s) zebrafish. Prior to embedding, fish were anaesthetized with cold AFW. Animals were then embedded in 1% (for 3-6dpf) and 2% (for 21dpf) low-melting-point agarose (LMP, Fisher Scientific) in a recording chamber (Fluorodish, World Precision Instruments). Low-melting-point agarose solidified for 20min, and the section covering the nose was carefully removed to expose the nostrils. The animal was then placed under the microscope with constant perfusion of AFW bubbled with carbogen (95% O2 and 5%CO2). First, spontaneous activity was measured for 30min. Afterwards, 5 repetitions of sensory stimuli (red light flash or food odour) were applied. The food odour stimulus was prepared by adding 1g of standard dried fish food (Zebrafeed, Sparos, <100), in 50ml of AFW, dissolved for 1hr and filtered with a 22μm filter and diluted 1:50 in AFW. For skin extract [119], an adult zebrafish was euthanized in ice-cold water, decapitated and the skin was peeled off from the body and incubated in 1 ml of AFW, mixed and centrifuged at 1300rpm and 4°C for 1h. 1 mL of the supernatant was then dissolved in 300 mL of AFW. Amino acids mixture [120] contained arginine, asparagine, aspartic acid, alanine, phenylalanine, histidine and methionine, all diluted in AFW at 10-4 mol/L final concentration. Ammonium chloride was diluted in AFW at 10-4 mol/L final concentration. The odour stimulus was delivered for 5sec through a tube positioned in the front of the fish, connected to an Arduino Due-controlled HPLC injection valve (Valco Instruments). Fluorescein (10-4M) was dissolved in AFW and used to measure the precise onset of odour delivery to the nose at the end of each experiment. For the light stimulus we used a red LED (LZ1-00R105, LedEngin; 625 nm wavelength) and placed it in the front of the recording chamber near the tube. The light stimulus was a flash of 2s duration with an intensity of 0.318 mW. Mechanical vibrations were delivered via solenoid tapper (SparkFun Electronics, ROB-10391), via 50 milliseconds application of 6Volts. Mild electric stimulation was delivered by tungsten electrodes that passed 1kHz oscillating current of 0.05 mA for a period of 1 second. The recordings were performed with a two-photon microscope (Scientifica) using a 16x water immersion objective (Nikon, NA 0.8, LWD 3.6). A mode-locked Ti:Sapphire laser (MaiTai Spectra-Physics) tuned to 920nm was used for excitation. Volumetric recordings (8 planes with Piezo) were obtained at an acquisition rate of 31.9Hz for a volume of 1536x512 pixels x 8 planes. Total duration of the recordings was 45-60min.

Juvenile zebrafish electrophysiological recordings of habenular neurons

The experiments were conducted in a juvenile zebrafish brain explant preparation [112]. Juvenile zebrafish were euthanized by immersion in ice-cold water, followed by decapitation to ensure death. The head was transferred in cold artificial cerebrospinal fluid (ACSF) bubbled with carbogen (95% O2/5% CO2). The ACSF [120] was composed of the following chemicals diluted in reverse-osmosis purified water: 131 mM NaCl, 2 mM KCl, 1.25 mM KH2PO4, 2 mM MgSO4.7H2O, 10 mM glucose, 2.5 mM CaCl2 and 20 mM NaHCO3. The eyes, jaws and ventral part of the skull were carefully removed using forceps, exposing the habenula. The brain explant was then affixed using tungsten pins to a small petri dish coated with Sylgard (World Precision Instruments) and perfused in constant flow bubbled ACSF.

We performed intracellular recordings of single habenular neurons, via borosilicate patch pipettes (10-12MOhm) mounted on a MultiClamp 700B amplifier. Electrodes contained the intracellular solution (in mM: 130 k-gluconate, 10 Na-gluconate, 10 HEPES, 10 Na2+-Phospho-Creatine, 4 NaCl, 4 ATP-Mg and 0.3 Na3+-GTP) [120] Negative voltage steps (-30mV) of 500ms were applied to measure the input resistance.

In vivo birthdating of neurons

Prior to injections, 2.5dpf larvae were dechorionated manually and anaesthetized in 0.01% MS-222 in AFW for 5-10min. Injections were done on larvae embedded in 1% low-melting point agarose in AFW and 0.01% MS-222 in AFW. The stock solution contained 5mM CellTracer Far-Red-AM or CellTracer CFSE Cell Proliferation Kit (Thermofisher) dissolved in DMSO provided with the proliferation kit. The injection mixtures contained 0.5μl of this CellTrace Far Red/ DMSO stock solution dissolved in 2.5μl of artificial cerebrospinal fluid (aCSF) with a final concentration of 1mM. The aCSF contained the following: 124 mM NaCl, 22 mM D-(+)-Glucose, 2.0 mM KCl, 1.6 mM MgSO4 · 7 H2O, 1.3 mM KH2PO4, 24 mM NaHCO3, 2.0 mM CaCl2 · 2 H2O. The injection needles were pulled with a Sutter Instrument Co. Model P-2000, from thin-walled borosilicate capillaries (1.00 mm; VWR), with the following settings: heat = 785, filament = 4, velocity = 40, delay = 220, pull = 70. The needle tip was cut open with forceps afterwards and a pressure injector (Eppendorf Femtojet 4i) was used to inject 1 nL of solution in the telencephalic ventricle near habenula of either 2,5 or 5 days old zebrafish larvae [102]. The pressure and time used for the injection were calibrated for each needle using a 0.01 mm calibration slide for microscopy. Usually, the pressure ranged between 100-150 hPa and the time span of the pressure pulse lasted for 0.30 – 0.70 s. After injection, fish were released from agarose and recovered at 28°C AFW and transferred to the fish facility and raised until 12 or 21 days.

21dpf fish were prepared for confocal microscopy imaging as described above for two-photon calcium imaging. Imaging was performed using a Zeiss Examiner Z1 confocal microscope with a 20x water-immersion objective (Zeiss, NA 1.0, Plan-Apochromat) at room temperature and constant perfusion of AFW bubbled with carbogen (95% O2 and 5% CO2). In vivo calcium recordings of the spontaneous activity in habenula were acquired at an acquisition rate of 1.918Hz for 512x1024pixels during 5min.

Data Analysis

Two-photon microscopy images were aligned using an adapted algorithm [121] that corrects for occasional drift in the XY dimension, based on "hierarchical model-based motion estimation [122]. Every recording was manually checked for motion and corresponding frames were discarded from further analysis. Individual neurons were semi-automatically detected using a pattern recognition algorithm as previously described [81, 112, 121]. Once neurons were detected, their locations were individually tracked during the recording. If any z-motion drift or if some detected neurons were no longer visible those neurons were discarded from further analysis. The pixels belonging to each neuron were then averaged providing the complete time course of each neuron over time. Same cell-detection algorithms were used for the confocal recordings in Figure 6. To distinguish between developmentally tagged and untagged neurons, we manually identified the red cells. To normalize the spontaneous activity for each cell to its baseline fluorescence, we calculated the fractional change in fluorescence ($\Delta F/F$) relative to the baseline, which was calculated as the 8th percentile of activity observed within 2min time window as previously described [95]. Clustering of neurons was performed as previously reported based on the k-means clustering algorithm in MATLAB as well as the calculation of cluster fidelity and cluster selectivity for sensory and tagged cells [81].

Prior to event detection, traces from neurons in the two-photon recordings were resampled to a final rate of 2 Hz (using decimate function in MATLAB), to match the sampling rate with confocal experiments. Significant calcium events were detected using an algorithm [95] that detects calcium events significantly different from noise level within a 95% confidence interval. A cell was considered active if at least one event was detected in 4min of ongoing activity. The amplitude of events was defined as the maximum peak in the event. The average activity per cell was defined as the sum of the area under the curve (using trapezoidal numerical integration method, function 'trapz' in MATLAB) for all events within one neuron. The fractional change in fluorescence ($\Delta F/F$) for the odour and light stimulus as well as mechanical vibrations and mild-electric stimulus was calculated by subtracting the average baseline fluorescence before stimulus onset (5sec) from the responsive window (10 seconds for odour, 2 seconds for light, mechanical vibrations and mild-electric stimulus from the onset of the stimulus). Cells were classified as responding if at least 4 out of 5 trials showed the same sign difference (+/-) locked to the stimulus onset. Only the positively responding neurons were taken into account for further analysis.

The focality index was calculated as 1 minus the average of the Euclidean distances between the top 10% neurons (with highest frequencies or durations) divided by the average of the Euclidean distances of all neurons within each hemisphere. The average focality index per fish was calculated by taking the average over the two hemispheres. Same focality index was calculated for the sensory-responding cells. Cluster fidelity was calculated by measuring the probability of pairs of neurons being in the same cluster during two different time periods [81]. As a control, we shuffled the cluster identity of neurons randomly.

To calculate cluster selectivity, we first calculated the cluster identity of each neuron using k-means clustering of spontaneous neural activity[81]. Later

we identified neurons with a given property, in this case either sensory responding neurons (Figure 4G), or developmentally tagged neurons (Figure 6L) and measured the sparseness in the distribution of identified neurons into clusters[81]. We then compared this to all and/or equal number of non-sensory responding neurons within each fish. If sparseness is 1 all identified neurons are selectively member of a single cluster, if sparseness is 0 all identified neurons are equally distributed into all functional clusters identified by k-means clustering.
The lateralization index was calculated as the difference between the percentage of responding neurons in left and right hemispheres.
In the confocal microscopy functional imaging, results for frequency, duration, number of active neurons, average activity and pairwise correlations, are shown for all planes imaged in each fish, as these recordings were done at different timepoints.

Quantification and Statistical Analysis
Statistical analysis was done using MATLAB and p-values are indicated in the figure legends (*$p<0.05$, **$p<0.01$, ***$p<0.001$). Student t-test was used for paired data and unpaired t-test when data was obtained from two independent datasets. For the data that displayed no Gaussian distribution, we used Wilcoxon signed rank test for paired data and Wilcoxon ranksum test for unpaired data.

Data and software availability
All analysis was performed with Fiji and MATLAB as indicated in the results section. All custom MATLAB scripts are available upon request.

SUPPLEMENTARY FIGURES

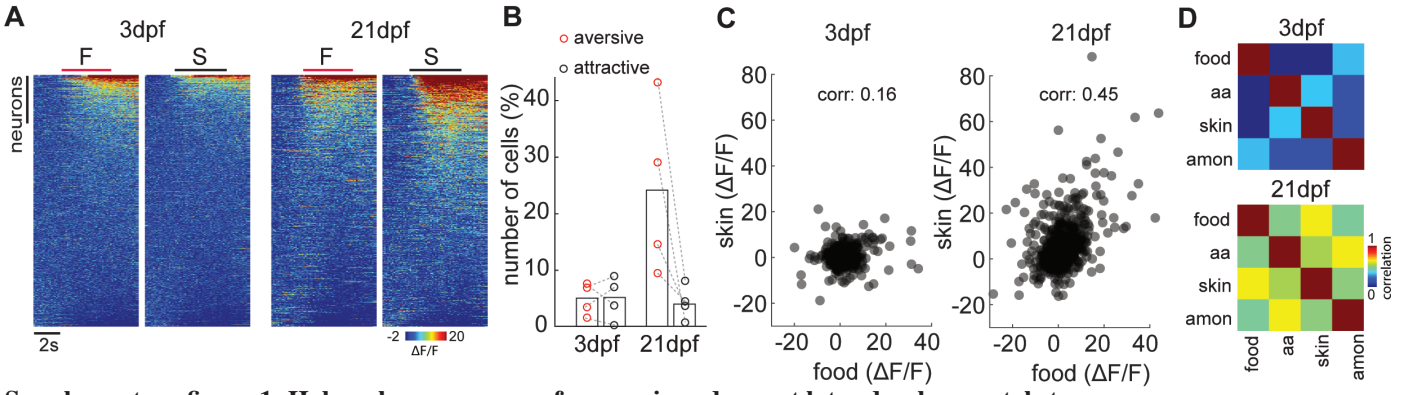

Supplementary figure 1: Habenular neurons prefer aversive odours at later developmental stages.
(A) Colour coded odour responses (ΔF/F) of all individual habenular neurons exposed to 10s of food odour and skin extract at 3dpf (n=4 fish, 208 ±25 neurons per fish) and 21 dpf (4 fish,283±107 neurons per fish). Black bars represent 100 neurons. (B) Percentage of neurons responding to aversive (red) vs attractive (black) odours at 3 and 21dpf. Note that the ratio habenular neurons responding to aversive odours is higher, at all 21dpf zebrafish. (C) Skin extract vs food odour response amplitude of all habenular neurons at 3 and 21dpf. Correlations between different stimulus representations by habenular responses are represented by "corr". (D) Correlation matrices representing pairwise Pearson's correlations among habenular responses to two attractive (food odour, aminoacids) and two aversive (skin extract, ammonia) odours at 3dpf (594 neurons) and 21dpf (925 neurons). All data presented as mean ±SEM.

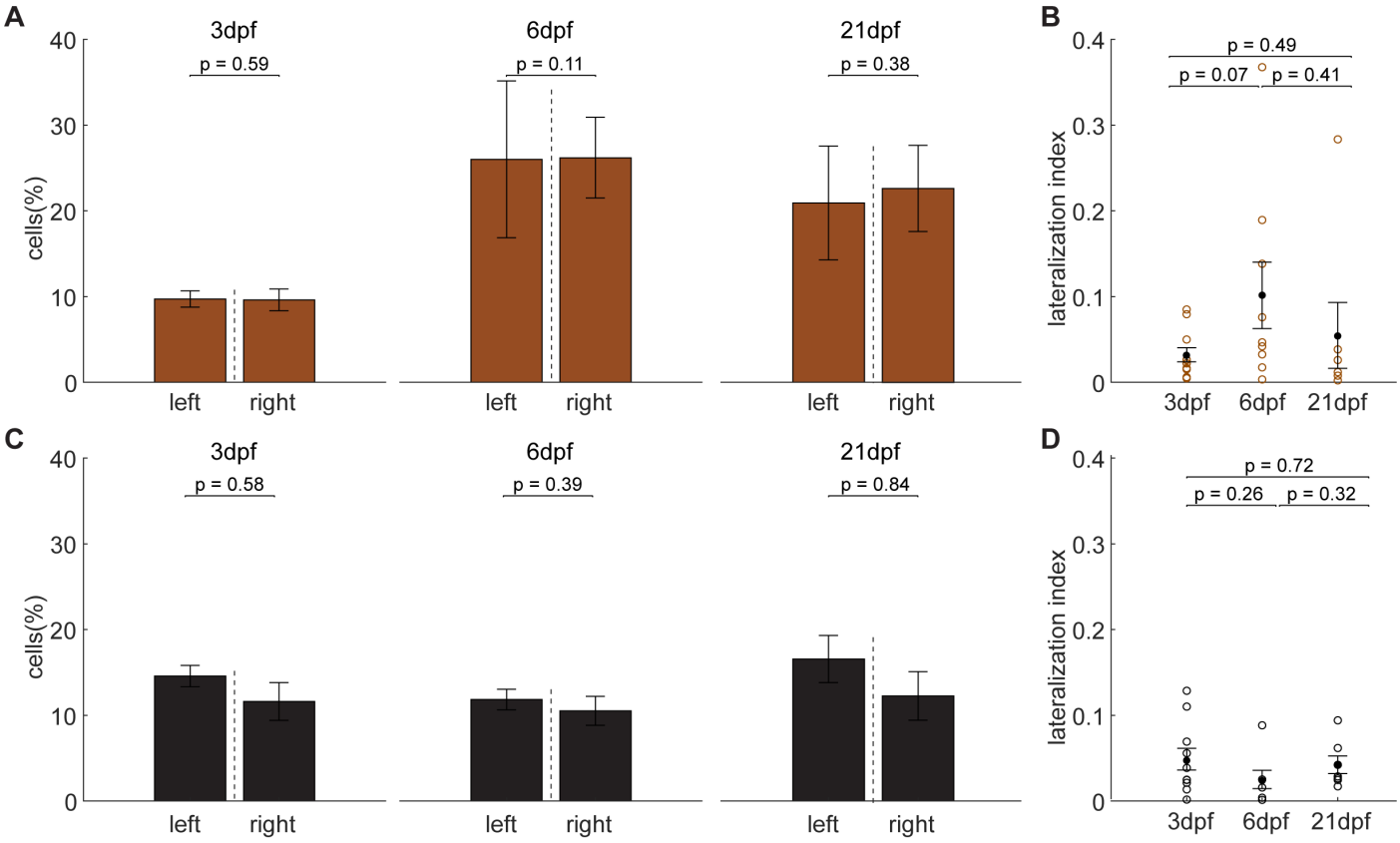

Supplementary figure 2: Mild-electric stimulus and mechanical vibrations evoke nonlateralized responses in habenula at all ages.
(A) The ratio of neurons responding to mild-electric stimulation in left vs right habenular hemispheres in 3dpf (n=11), 6dpf (n=9) and 21dpf (n=7) zebrafish. Wilcoxon signed-rank test. (B) Average lateralization index of the habenular responses to mild electric stimulus at 3, 6 and 21dpf zebrafish. Wilcoxon ranksum test. (C) The ratio of neurons responding to mechanical vibrations in left vs right habenular hemispheres in 3dpf (n=11), 6dpf (n=9) and 21dpf (n=7) zebrafish. Wilcoxon signed-rank test. (D) Average lateralization index of the habenular responses to mechanical vibrations at 3, 6 and 21dpf zebrafish. Wilcoxon ranksum test. All data presented as mean ±SEM.

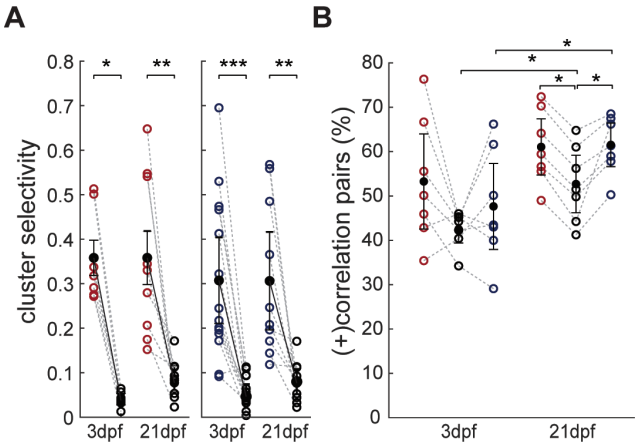

Supplementary figure 3: Odour and light responsive habenular neurons overlap with the distinct functional clusters with correlated spontaneous activity

(A) Cluster selectivity, depicting how odour (red) or light (blue) responding neurons are distributed into functional clusters based on their spontaneous activity. High selectivity means that both odour and light responding neurons belong to fewer clusters compared to all nonsensory neurons (grey dots), at 3 and 21dpf. (B) The ratio of neural pairs with significant ($p<0.05$) positive correlations of spontaneous activity, for odour (red) and light (blue) responsive neurons, when compared to all non-sensory (grey) neurons, at 3 and 21dpf. *$p<0.05$, **$p<0.01$, ***$p<0.001$, Wilcoxon signed-rank test for paired comparisons and Wilcoxon ranksum test for unpaired comparisons. All data presented as mean ±SEM.